processes

MDPI

Review

Gas Dispersion in Non-Newtonian Fluids with Mechanically Agitated Systems: A Review

Paloma Lins Barros, Farhad Ein-Mozaffari * and Ali Lohi

Department of Chemical Engineering, Ryerson University, 350 Victoria Street, Toronto, ON M5B 2K3, Canada; paloma.barros@ryerson.ca (P.L.B.); alohi@ryerson.ca (A.L.)
* Correspondence: fmozaffa@ryerson.ca

Abstract: Gas dispersion in non-Newtonian fluids is encountered in a broad range of chemical, biochemical, and food industries. Mechanically agitated vessels are commonly employed in these processes because they promote high degree of contact between the phases. However, mixing non-Newtonian fluids is a challenging task that requires comprehensive knowledge of the mixing flow to accurately design stirred vessels. Therefore, this review presents the developments accomplished by researchers in this field. The present work describes mixing and mass transfer variables, namely volumetric mass transfer coefficient, power consumption, gas holdup, bubble diameter, and cavern size. It presents empirical correlations for the mixing variables and discusses the effects of operating and design parameters on the mixing and mass transfer process. Furthermore, this paper demonstrates the advantages of employing computational fluid dynamics tools to shed light on the hydrodynamics of this complex flow. The literature review shows that knowledge gaps remain for gas dispersion in yield stress fluids and non-Newtonian fluids with viscoelastic effects. In addition, comprehensive studies accounting for the scale-up of these mixing processes still need to be accomplished. Hence, further investigation of the flow patterns under different process and design conditions are valuable to have an appropriate insight into this complex system.

Keywords: mixing; gas dispersion; gas holdup; non-Newtonian fluids; mass transfer coefficient

check for updates

Citation: Lins Barros, P.; Ein-Mozaffari, F.; Lohi, A. Gas Dispersion in Non-Newtonian Fluids with Mechanically Agitated Systems: A Review. *Processes* **2022**, *10*, 275. https://doi.org/10.3390/pr10020275

Academic Editor: Václav Uruba

Received: 5 December 2021
Accepted: 27 January 2022
Published: 30 January 2022

1. Introduction

Multiphase flow operations have been extensively investigated due to their wide industrial applications [1–5]. These operations are often evaluated by considering the degree of contact between the phases. For instance, the phases interaction is crucial to determine the performance of multiphase mixing processes. In view of that, stirred vessels are commonly utilized for multiphase mixing operations due to their versatility in promoting adequate mixing characteristics for different types of fluids. For gas-liquid mixing, for example, high mass transfer coefficients can be achieved when employing sparged agitated vessels [6]. Hence, many studies have investigated these mixing systems, especially with regard to gas dispersion in Newtonian fluids [7–10]. Although fewer studies refer to the aeration of non-Newtonian fluids, a broad range of industrial applicability can still be observed in food, chemical, biochemical, pulp and paper, and painting industries [11]. More specifically, gas dispersion in non-Newtonian fluids with shear-thinning characteristics can be encountered in antibiotic and polysaccharide production, fungal fermentation, wastewater treatment, and cell culture [12–16].

The aeration and mixing of non-Newtonian fluids have many challenges especially because of their complex rheological characteristics. Since the viscosity varies depending on the local shear rate, poor mixing regions may exist, which can lead to process inefficiencies [17]. Thus, impeller configurations in aerated non-Newtonian applications are often designed to target the reduction of stagnant regions created by the shear rate gradient in the vessel and to enhance the mixing performance [18]. Some of the mixing configurations

are comprised of a single impeller [15,19–21], multiple impellers on the same shaft [22,23], side-entering impellers [24], angled-shaft impellers [25], planetary mixers [26], and coaxial mixers [27–30]

Furthermore, the mixing and mass transfer performance of these gas-liquid systems is a result of a complex interaction between the phases that depends on multiple variables, such as the design parameters, operating conditions, and physical properties of the phase's components [31]. The main variables to assess the mixing and mass transfer behavior are power consumption [32], gas holdup [29,33], mixing time [22,34], bubble size [35], and volumetric mass transfer coefficient [36,37]. The complex gas dispersion phenomenon in non-Newtonian fluids also requires information on the cavity structures [16], flow regime [19], and cavern size [38].

In view of that, this work aims to provide a comprehensive literature review on the gas dispersion in non-Newtonian fluids using stirred vessels in which the significant challenges are presented and the effect of agitation, aeration, and rheological properties on the mixing performance are discussed. Also, the main available approaches for evaluating these mixing and mass transfer parameters are presented, namely empirical correlations, experimental techniques, and numerical modeling.

This review presents important mixing and mass transfer characteristic values, measurement techniques, and empirical correlations in Section 2. The effects of agitation (i.e., impeller type, configuration, and rotation speed) on the characteristic parameters are addressed in Section 3. Section 4 brings together the important findings regarding the aeration effect on the mixing and mass transfer performance. The findings and significant concerns about the rheological effects on the gas dispersion in non-Newtonian fluids are included in Section 5. Section 6 discusses the advantages of using computational fluid dynamics (CFD) in evaluating the hydrodynamics of such a complex system, and also presents important closure models used by previous researchers. Section 7 discusses the potential application of coaxial mixers for the gas dispersion in yield-pseudoplastic fluids and compares the performance of a coaxial mixer to that of a single impeller. Section 8 presents scale-up strategies available in the literature for gas dispersion in non-Newtonian fluids and briefly discuss the most common challenges encountered during the scale-up of these mixing systems. In Section 9, final considerations are presented and some suggestions for future work are highlighted.

2. Characterization of Gas Dispersion in Non-Newtonian Fluids

2.1. Power Consumption

Power consumption is a relevant variable to assess the mixing performance since it is directly related to the cost of operation. For non-Newtonian media, a significant amount of energy is required to overcome the poor mixing, and for some cases, it represents the main source of operational cost [33].

Due to the complex phenomena in the mixing system, it is difficult to have a general empirical correlation to estimate the gassed fluid's power consumption. Table 1 presents several empirical correlations that were proposed or verified in the literature to calculate the gassed power consumption in aerated non-Newtonian fluids. For instance, Luong and Volesky [39] studied the aeration in different pseudoplastic solutions of carboxy-methyl cellulose (CMC) dissolved in water and observed that a correlation for gas dispersion in Newtonian fluids can be applied using different fitted parameters. Gomez-Dias and Navaza [40] evaluated a gas-liquid mixing system containing power-law fluids using the correlation proposed by Michel and Miller [41], in which the values of the constants depend on the impeller geometry. Both studies from Luong and Volesky [39] and Gomez-Diaz and Navaza [40] have used the form of the correlations originally proposed for Newtonian fluids. However, this consideration only applies to solutions with low polymer concentration, in which the effects of high shear-thinning behavior on the power consumption can be neglected. Gabelle et al. [22] included the impeller type and vessel geometry effects on the estimation of the gassed power uptake for CMC and xanthan gum solutions described by

the power law model. They considered different scales and multiple impeller configurations by proposing a novel expression in terms of the gas flow rate, tank diameter, impeller diameter, and power number of the stirrer closer to the sparger. The empirical correlation proposed by Gabelle et al. [22] accounts for a wide variation in design and, as a result, prediction errors are more likely to occur when using this expression. This is the reason why a very specific range of process conditions needs to be defined to obtain empirical correlations with better accuracy. Xie et al. [42] obtained the model fitted parameters for each combination of impellers in their triple-impeller configuration for gas dispersion in high shear-thinning xanthan gum solutions. They observed that the correlation including Reynolds number, Froud number, and flow number gave a better prediction for most of the configurations even when varying the xanthan gum concentration in an aqueous solution. Jamshidzadeh et al. [32] verified different correlations for gas dispersion in a power-law fluid using coaxial mixers, which are comprised of a high-speed central impeller and a close clearance impeller rotating slowly. They obtained different fitted parameters for each pumping direction including the effect of both co-rotation and counter-rotation modes. Although dimensionless correlations as obtained by Xie et al. [42] and Jamshidzadeh et al. [32] are important to account for the effect of crucial parameters, a detailed methodology based on a dimensional analysis for gas dispersion in non-Newtonian fluids is still missing. For example, the Buckingham π theorem is able to define the number of independent dimensionless groups that mathematically characterize a response variable.

Table 1. Empirical correlations for power consumption of gassed non-Newtonian fluids.

Correlation	Aeration Range	Fluid Type	Impeller Type	Agitation (rps)	Reference
$ln\left(\frac{P_g}{P_u}\right) = -15.36\, Q^{0.62}\, T^{-1.7}\left(\frac{D}{T}\right)^{0.51} P_o^{0.16}$	0.0039–0.0078 m/s	Air-xanthan gum solutions Air-CMC solutions (Conc. = 0.25–0.5 wt%)	Double impeller (RT, PBTD, Mixel TT)	8.3 in small vessel and 5 in large vessel	[22]
$\frac{P_g}{P_u} = c_1 Re^{c_2} Fl^{c_3}$ $\frac{P_g}{P_u} = c_1 Fr^{c_2} Fl^{c_3}$ $\frac{P_g}{P_u} = c_1 Re^{c_2} Fr^{c_3} Fl^{c_4}$	0.1–0.2 vvm	Air-CMC solutions (Conc. = 0.5–1.5 wt%)	Anchor-Double PBD and Anchor-Double PBU	$N_a = 0.17$–0.5 $N_c = 2.3$–47	[32]
$\frac{P_g}{P_u} = 0.514(Fl)^{-0.38}(We)^{-0.194}$	0.860–1.581 vvm	Air-CMC solutions (Conc. = 0.2–0.67 wt%)	Six-blade turbine	9.6–14.28	[39]
$P_g = 0.706\left(\frac{P_u^2 N D^3}{Q^{0.56}}\right)^{0.4}$	18–36 dm^3/h	CO2-CMC solution (Conc. = 0.5–10 g/dm^3) CO2-Alginate solution (Conc. = 0.5–1.5 g/dm^3)	Rushton turbine	3.3–10	[40]
$\frac{P_g}{P_u} = c_1 Re^{c_2} Fr^{c_3}$ $\frac{P_g}{P_u} = c_1 Re^{c_2} Fr^{c_3} Fl^{c_4}$	0.5–1 vvm	Air-xanthan gum solutions (Conc. = 1–3 wt%)	Triple impeller (RT, HBT, WHD, WHU, EG, DHR)	1.67–11.67	[42]

Furthermore, the power consumption of a gassed stirred system can be obtained from torque measurements as given by Equation (1) for single shaft impellers [20] or Equation (2) for coaxial mixers [30]:

$$P_g = 2\pi N M \tag{1}$$

$$P_g = 2\pi N_C M_C + 2\pi N_A M_A \tag{2}$$

where N is the impeller speed, and M is the corrected torque, which is calculated by subtracting the friction torque (i.e., the torque measured in a vessel prior to filling it with the fluids to be evaluated) from the actual measured value (Equation (3)):

$$M = M_{measured} - M_{friction} \tag{3}$$

2.2. Gas Holdup

Gas holdup is the volume fraction of the dispersed gas in the system, which is the ratio between the volume occupied by the bubbles and the total bulk volume. In order to

improve mass transfer in an aerated process, a high overall gas holdup is desired, along with a good distribution of the bubbles throughout the liquid phase. Therefore, both global and local gas holdup measurements should be obtained to adequately assess the mixing system [29]. Several experimental techniques are available to measure the gas holdup, such as the visual method [35], optical probe [43], vision probes [44], electric conductivity probe [45], particle image velocimetry [46], γ-ray computer tomography [47], and electrical resistance tomography [48,49]. Although the experimental methods used for measuring the gas holdup in Newtonian fluids can be employed, it is important to consider the particularities of the non-Newtonian fluid, such as the degree of opacity, in order to choose a suitable experimental technique [50].

Table 2 presents empirical correlations available in the literature to estimate the gas holdup in non-Newtonian fluids, followed by its estimated range depicted in Figure 1. The expressions were fitted based on global information of the gas holdup, and it does not bypass the requirement to analyze local gas holdup values in order to have a better insight into the gas dispersion inside the vessel. Machon et al. [51] employed the visual method to investigate the global gas holdup using different CMC solutions for the aeration rates up to 1 vvm. The proportionality constant in their empirical correlation depends on the CMC concentration. Garcia-Ochoa et al. [14] modified the correlation proposed by Kudrewizki and Rabe [52] in order to consider the viscous force effect and employed this correlation for the xanthan gum fermentation, which consists of a rheological evolving system. Khalili et al. [20] proposed a correlation for a yield stress fluid by fitting the parameters for a single ASI impeller and taking into account the variation of impeller speed, aeration rate, and xanthan gum concentration. Jamshidzadeh et al. [49], in turn, measured the gas holdup through electrical-resistance tomography and proposed correlations for the gas dispersion in power-law fluids using coaxial mixers in the co-rotation mode. Their correlation considered the variation in the speed ratio (rotational speed of the central impeller/rotational speed of the anchor impeller), apparent fluid viscosity, and aeration rate between 0.1 to 0.2 vvm. In theory, these correlations should be applied to all design and operating conditions within the range studied in each work. However, some deviations can be observed especially if a different technique for gas holdup measurement is employed. Overall, a good practice is to use the general form of a correlation that includes all independent variables to be investigated in a case study and use a new experimental dataset to find the best fitting parameters. Hence, when applying the desired range of process conditions, the best fit of the empirical model can be obtained to accurately predict the gas holdup. In addition, the development of dimensionless correlations is useful to account for the effect of agitation and aeration phenomena in such a complex multiphase system, as well as for the scale-up study keeping a certain mixing behavior constant.

2.3. Volumetric Mass Transfer Coefficient

The volumetric mass transfer coefficient (k_La) is used to assess the mass transfer in aerated systems and is commonly used for scale-up purposes [53]. Many authors have suggested different experimental techniques and empirical correlations to measure or estimate this parameter [54,55]. As reviewed by Gogate and Pandit [54] and Pinelli et al. [56], some of the experimental methods are the dynamic method [57], dynamic pressure method [36,58], simplified dynamic pressure method [59], and dynamic start-up method [22]. In addition, steady-state methods such as the sodium sulfite oxidation method [60,61] are available to measure the volumetric mass transfer coefficient based on the chemical reaction in the vessel [62,63]. Despite all these available experimental methods, special care must be taken when measuring the volumetric mass transfer coefficient in non-Newtonian systems with microorganisms. In these cases, the experimental technique must not interrupt the oxygen supply and the environment must be adequate for the respiring cells [36].

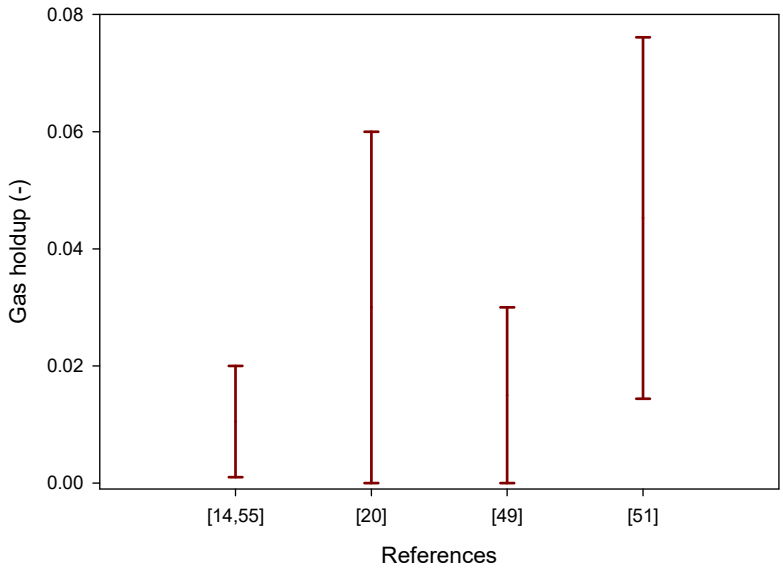

Figure 1. Range of gas holdup estimated from empirical correlations for gas dispersion in non−Newtonian fluids.

Table 2. Empirical correlations for gas holdup of stirred non-Newtonian fluids.

Correlation	Aeration Range	Fluid Type	Impeller Type	Agitation (rps)	Reference
$\frac{\varepsilon_g}{1-\varepsilon_g} = 0.819\frac{v_s^{\frac{2}{3}} N^{\frac{2}{5}} T^{\frac{4}{15}}}{g^{\frac{1}{3}}}\left(\frac{\rho_L}{\sigma}\right)^{\frac{1}{5}}\left(\frac{\rho_L}{\rho_L-\rho_g}\right)\left(\frac{\rho_L}{\rho_g}\right)^{-\frac{1}{15}}\left(\frac{\mu_L}{\mu_g}\right)^{-1/4}$	0.001–0.01 m/s	*Xanthomonas campestris* culture (μ_{ap} = 0.001–0.02 Pa·s)	Double disk turbine	2–10	[14,55]
$\varepsilon_g = 0.0412(Fl)^{0.39}(\mu_{ap})^{-1.47}$	0–0.0008 m^3/s	Air-xanthan gum solutions (Conc. = 0.5–1 wt%)	ASI	0–6	[20]
$\varepsilon_g = 0.00002\left(\frac{P_g}{V}\right)^{0.728} v_s^{0.485} N_R^{0.386} \mu_{ap}^{0.154}$	0.1–0.2 vvm	Air-CMC solutions (Conc. = 0.5–1 wt%)	Anchor-Double PBD	N_C = 2.55–5.2 N_A = 0–0.5	[49]
$\varepsilon_g = 0.00085(f_{Pc}N_c + f_{Pa}N_a)^{1.371} v_s^{0.466} N_R^{0.127} \mu_{ap}^{0.301}$ $\varepsilon_g = 0.00639(N_c D_c)^{1.664} v_s^{0.490} N_R^{0.255} \mu_{ap}^{0.375}$					
$\varepsilon_g = c_1\left(\frac{P}{\rho_L V}\right)^{0.3} v_s^{0.7}$	0.25–1 vvm	Air-CMC solutions (Conc. = 0.5–1 wt%)	Rushton turbine	3.3–7.3	[51]

Table 3 presents empirical correlations reported in the literature to estimate the volumetric mass transfer coefficient. Garcia-Ochoa et al. [64] studied the xanthan gum fermentation and obtained different correlations considering the effect of operating conditions and fluid viscosity, in which the constants of proportionality were determined according to the rheological model of the fluid. For a similar empirical correlation, Gomez-Dias and Navaza [40] obtained model fitted parameters for each fluid type in their study. Gabelle et al. [22], in turn, proposed a correlation that considers different tank sizes and impeller types in a double impeller configuration. Their model was compared to other correlations in the literature, and an average error was observed within 20% to 31%. It is worth mentioning, however, that small differences are expected when using different experimental methods to measure the volumetric mass transfer coefficient. Furthermore, Jamshidzadeh et al. [37] proposed novel dimensional and dimensionless correlations for coaxial mixers. The parameters were fitted for an impeller configuration in co-rotation mode, and they found that the best correlation should include the effects of both apparent viscosity and speed ratio. The parameters for the dimensionless correlations were fitted for the anchor-double PBT coaxial mixer, whereas different parameters for the dimensional correlations were obtained for the anchor-double PBT and the anchor-double Scaba coaxial mixers. Although the proposed correlations in Table 3 were designed to calculate the average volumetric mass transfer

coefficient of the process, they were fitted using local data. Hence, these correlations are more likely to truly represent the actual k_La data in systems where homogeneous shear stress and homogeneous gas-liquid mixing throughout the vessel can be observed. Due to the nature of shear-thinning fluids, a higher mass transfer coefficient is measured near the impeller as a result of the higher impeller rotation speed and thus a lower apparent viscosity around the impeller. Therefore, more accurate correlations are obtained by analyzing the k_La in different parts of the vessel to account for the non-Newtonian behavior.

Table 3. Empirical correlations for volumetric mass transfer coefficient of gassed non-Newtonian fluids.

Correlation	Aeration Range	Fluid Type	Impeller Type	Agitation (rps)	Reference
$k_La = 0.023\left(\frac{P_g}{V}\right)^{0.44} v_s^{0.47}\left(1+\frac{\mu_{ap}}{0.018}\right)^{-1}$	0.0039–0.0078 m/s	Air-xanthan gum solutions Air-CMC solutions (Conc. = 0.25–0.5 wt%)	Double impeller (RT, PBTD, Mixel TT)	8.3 in small vessel and 5 in large vessel	[22]
$k_La = c_1(N_cD_c)^{c_2} v_s^{c_3} N_p^{c_4} R_N^{c_5}$ $k_La = c_1(N_cD_c)^{c_2} v_s^{c_3} \mu_{ap}^{c_4} R_N^{c_5}$ $k_La = c_1(N_cD_c)^{c_2} v_s^{c_3} \mu_{ap}^{c_4}$ $\frac{k_La\,D_c^2}{D_L} = 485.984\left(\frac{\rho N_c D_c^2}{\mu}\right)^{0.242}\left(\frac{N_cD_c}{v_g}\right)^{-0.568}\left(\frac{\rho N_c^2 D_c^3}{\sigma}\right)^{0.854}$	0.1–0.2 vvm	Air-CMC solutions (Conc. = 0.5–1.5 wt%)	Anchor-Double PBD Anchor-Double Scaba	$N_a = 0.17$–0.5 $N_c = 2.3$–47	[37]
$k_La = c_1\left(\frac{P_{eff}}{V}\right)^{C_2} v_g^{c_3} \mu_{ap}^{c_4}$	18–36 dm^3/h	CO2-CMC solution (Conc. = 0.5–10 g/dm^3) CO2-Alginate solution Conc. = 0.5–1.5 g/dm^3)	Rushton turbine	3.3–10	[40]
$\frac{k_La\,D^2}{D_L} = c_1(Re)^{\frac{1}{2}}\left(\frac{ND}{v_s}\right)^{-\frac{1}{2}}(We)$ $k_La = c_1 N^2 v_s^{1/2} \mu_{ap}^{-1/2}$ $k_La = c_1\left(\frac{P_g}{V}\right)^{0.6} v_g^{1/2} \mu_{ap}^{-1/2}$	0.4–1 vvm	*Xanthomonas campestris* culture	Double disk turbine	3.5–15.81	[64]

2.4. Bubble Mean Size

Information on the bubble size distribution gives a detailed analysis of the interfacial area. High mass transfer requires a large interfacial area that can be achieved by decreasing the bubble mean diameter. However, the determination of the bubble size distribution is complex, and it is even more challenging in the non-Newtonian media [65]. In this case, the shear rate variation throughout the mixing system promotes a non-uniform bubble size distribution in which lower bubble mean sizes are observed near the impeller region due to higher shear rate in this region [66].

Some of the experimental techniques for measuring the bubble size employ conductivity probes [67,68], imaging probes [65,69], suction probes [66,70–72], particle image velocimetry [46], photography [51,73], laser-induced fluorescence [74], and gas disengagement technique [20,75]. The experimental techniques must be set accordingly to obtain the bubble size in different regions of the vessel to have a better representation of the wide bubble size distribution.

Table 4 presents empirical correlations available in the literature to estimate the mean bubble size in non-Newtonian fluids. Khalili et al. [20] studied the gas dispersion in pseudoplastic fluids with yield stress and employed an empirical correlation originally proposed by Calderbank [76], which assumes a balance between turbulent stresses and surface tension. Khalili et al. [20] used the dynamic gas disengagement technique combined with electrical resistance tomography to obtain the number of bubble classes and to get experimental data to calculate the bubble mean diameter. This technique is based on the dynamic measurement of the gas holdup after the aeration suppression, knowing that bubbles with different diameters disengage with different velocities [75]. However, it is important to mention that this method does not give entirely accurate results for high shear-thinning fluids, as small bubbles stay trapped in the liquid phase even after aeration stops.

In addition, Garcia-Ochoa et al. [14] estimated the bubble mean diameter in a rheologically evolving system, using a correlation that was originally proposed by Bhavaraju et al. [77] for Newtonian fluids. Momiroski et al. [65] obtained different proportionality constants for coalescing and non-coalescing systems with a pseudoplastic fluid for three impeller types. Bach et al. [34], in turn, correlated the bubble size to the superficial gas velocity and specific gassed power uptake, applying a constant of proportionality that depends on the aeration rate. Due to the challenges of measuring the bubble size in rheologically complex fluids, a high degree of uncertainty is expected when using these empirical correlations. Therefore, the measurement of the volumetric mass transfer coefficient is often preferred to draw conclusions about the mass transfer performance of the mixing system.

Table 4. Empirical correlations for mean bubble size in gassed non-Newtonian fluids.

Correlation	Fluid Type	Impeller Type	Reference
$d_{32} = 0.7 \frac{\sigma^{0.6}}{\left(\frac{P}{V}\right)^{0.4} \rho_L^{0.2}} \left(\frac{\mu_L}{\mu_g}\right)^{0.1}$	*Xanthomonas campestris* culture	Double disk turbine	[14]
$d_{32} = 4.15 \frac{\sigma^{0.6}}{\left(\frac{P_g}{V}\right)^{0.4} \rho_L^{0.2}} \varepsilon_g{}^{0.2} \left(\frac{\mu_g}{\mu}\right)^{0.25} + 9 \times 10^{-4}$	Xanthan gum solutions	Rushton disk turbine, ASI, and PBT	[20]
$d_{32} = c_1 (v_g) \left(\frac{P_g}{V}\right)^{-2.95}$	*Trichoderma reesei* fermentation using Xanthan gum solutions as model fluids	Hayward Tyler B2 impeller	[34]
$d_{32} = c_1 \left(\frac{\sigma^{\frac{3}{5}} \left(\frac{\mu_L}{\mu_G}\right)^{\frac{1}{10}}}{\rho_L^{\frac{1}{5}} \left(\frac{P_g}{V}\right)^{\frac{2}{5}}} \right)$	CMC solutions	Rushton turbine, Hollow blade turbine, and PBT	[65]

2.5. Flow Regimes

The flow regimes describe the degree of the bubbles' dispersion and its flow patterns in the agitated vessel [7]. The mixing efficiency and mass transfer are directly affected by the flow regime especially when the gas-liquid mass transfer is the limiting step [78,79]. The bubbles are dispersed in the mixing vessel via two mechanisms: agitation and aeration. The agitation promoted by the impeller's rotation defines circulation patterns inside the vessel. Depending on the aeration rate, the bubbles may follow the circulation pattern defined by the impellers rotation or may have a stronger ascending movement. The suitable bubble dispersion is achieved when the agitation mechanism is dominant. In this case, the gas phase enters the system through the sparger located below the impeller and flows according to the liquid flow pattern defined by the impeller type.

Three main flow regimes can be defined in terms of the pumping capacity and the relative buoyancy forces: flooding, loading, and complete dispersion [80]. The gas distribution in each flow regime is illustrated in Figure 2.

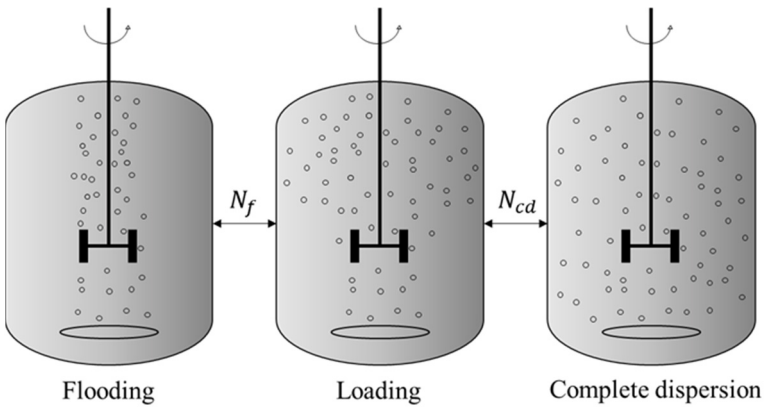

Figure 2. Gas-liquid flow regimes in agitated vessels.

The flooding regime occurs when the gas phase accumulates near the impeller region, resulting in poor bubbles dispersion and formation of oxygen-deficient regions. The loading regime is featured by gas dispersion above the impeller blades when the pumped liquid reaches enough radial velocity to disperse the gas away from the impeller vicinity. A completely dispersed regime, in turn, is highly desired. It refers to well-distributed gas bubbles throughout the entire vessel and significant gas recirculation to the impeller [6].

The prediction of regime transitions is essential from an industrial point of view [79]. It enables to define operating conditions that maximize mass transfer performance avoiding undesired flooding conditions. Some of the experimental methods available to identify the regime transitions are the visual observation method [81], optical probe method [7,78], and tomography methods [48,82]. Also, the flow regime transition can be identified based on global measurements of power consumption, volumetric mass transfer coefficient, or gas holdup curves [80,83,84]. However, previous knowledge about the behavior of global measurements upon varying flow regimes is expected.

Furthermore, the flow regimes are closely related to the cavitation phenomenon in stirred vessels because the cavity structures control the gassed power consumption, which affects the pumping capacity and further gas distribution [85]. Nienow [86] reported that stable cavities are formed in high viscous fluids. Therefore, a higher impeller speed and a lower sparging rate are required to avoid large cavities in these systems in order to achieve a higher degree of bubble dispersion, such as in loading or complete dispersion regimes [87,88]. For non-Newtonian fluids, the studies in the literature mainly address complete dispersed regimes by setting a suitable aeration rate and impeller speed [20–22]. Hassan et al. [89] and Jegatheeswaran et al. [30] studied aerated non-Newtonian systems in stirred vessels under loading and complete dispersed regime. Similarly, Khalili et al. [19] and Jamshidzadeh et al. [9] studied the transition between loading and complete dispersed regimes by determining the critical impeller speed for different impeller types used for gas dispersion in yield stress fluids and power-law fluids, respectively. Jegatheeswaran and Ein-Mozaffari [33] investigated the gas dispersion in power-law fluids using coaxial mixers and observed that the likelihood of a flooding regime surprisingly increases when increasing the anchor impeller speed to 50 rpm. This disruptive effect for high anchor speed was corroborated by Jamshidzadeh et al. [29], whose observations demonstrated that the flooding regime was achieved when the anchor speed increased up to 30 rpm. Jamshidzadeh et al. [32] focused their study on the complete dispersed regime but included some results for gas dispersion in power-law fluids under a flooding and loading regime ($Re < 800$). Despite the importance of investigating the flow regimes in non-Newtonian systems, scant studies are available in the literature aiming at investigating the flow regime transition or providing a detailed analysis of the mixing parameters considering all possible flow regimes.

2.6. Cavern Size

For non-Newtonian mixing systems, the determination of the cavern size is significant in verifying the performance of the agitator. In fact, cavern formation is observed in the presence of pseudoplastic fluids with yield stress [90,91]. The cavern is a well-mixed region that is formed due to the high shear rate induced by the impeller rotation [92]. An undesired stagnant region surrounds the cavern; therefore, increasing the cavern size is highly desired in the gas-liquid mixing system, which can be done by varying the impeller type and speed [92]. Most of the studies available in the literature to evaluate the cavern formation were conducted with single-phase mixing vessels [27,93,94]. Fewer works investigated the caverns in gas-liquid mixing systems. For instance, Yagi and Yoshida [95] visually observed a donut-shaped cavern region around the impeller in an aerated system. Solomon et al. [96] investigated the cavern formation using photographs and reported that smaller cavern sizes were obtained for aerated systems compared to unaerated vessels at the same impeller speed. Solomon et al. [96] also obtained a theoretical model to predict the cavern size for single and double impellers, as expressed in Equations (4) and (5), respectively. The

proposed model applies for both aerated and unaerated mixing vessels by considering the power number obtained for the operating conditions in the system.

$$log\left(\frac{r}{D}\right) = \frac{1}{3}log\left(P_oN^2\right) + \frac{1}{3}log\left(\frac{\rho D^2}{2\pi^3\tau_y}\right) \quad (4)$$

$$log\left(\frac{r}{D}\right) = \frac{1}{3}log\left(P_oN^2\right) + \frac{1}{3}log\left(\frac{\rho D^2}{4\pi^3\tau_y}\right) \quad (5)$$

where r is the cavern radius, D is the impeller diameter, P_o is the power number, ρ is the fluid density, and τ_y is the yield stress.

In addition, Moilanen et al. [97] investigated the gas dispersion in a yield-stress fluid using computational fluid dynamics (CFD), which enabled the prediction of the cavern formation within the vessel.

In industrial processes, the design parameters and operating conditions must be set to increase the size of the cavern. The cavern must reach the vessel wall and fluid surface in pseudoplastic fluids with yield stress to get a more homogeneous mixing in the vessel. The most straightforward way of addressing this issue is to employ an impeller configuration in which the minimum shear stress throughout the tank is higher than the fluid's yield stress. Also, although the upward gas movement is an additional source of shear stress, the aeration reduces the pumping capacity of the impeller, which decreases the power uptake and consequently reduces the shear rate. As a result, the detailed study of the two-phase flow hydrodynamics in the mixing vessel is even more crucial for non-Newtonian fluids under gassing condition.

3. Agitation Effect

The impeller plays the most important role in providing adequate gas dispersion in stirred vessels [98,99]. Overall, the impellers can pump the bulk flow axially, radially, or with a combination of both directions. Figure 3 illustrates the shape of typical impellers employed in mechanically agitated vessels. Table 5 summarizes the main research works that compared different impeller types and configurations. A more detailed analysis of the outcomes is demonstrated in the following sections, which also discuss the effect of the rotational speed on the performance of different mixing configurations.

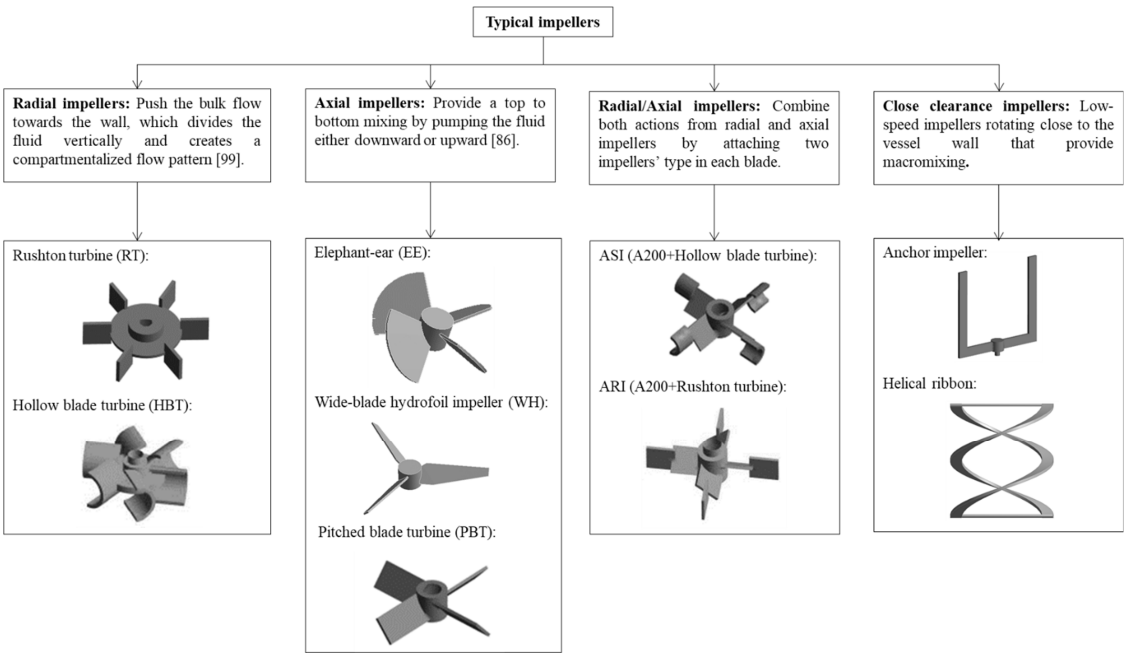

Figure 3. Different types of impellers.

Table 5. Remarks on different impeller types and configurations utilized for gas dispersion in non-Newtonian fluids.

Reference	System Studied	Impeller Configuration	Impeller Types	Pumping Direction	Remarks
[15]	Air-Activated Sludge (Power-law)	Single	ARI ASI RT	Axial/Radial Axial/Radial Radial	ASI showed a better gas-liquid mixing performance.
[18]	Air-Xanthan Gum (Power-law)	Coaxial	GT Paddle-Rushton GT Paddle-BDT6 GT Paddle-PBTD	Radial Radial Down Axial	The central impeller BDT-6 pro-moted the highest global volume fraction and RPD whereas PBTD promoted the highest k_La at a fixed power drawn.
[19]	Air-Xanthan Gum (Herschel-Bulkley)	Single	PBT DRT ASI	Down axial Radial Axial/Radial	ASI gave the most stable flow, promoted higher RPD upon gassing and more uniform shear rate distribution.
[29]	Air-CMC (Power-law)	Coaxial	Anchor-Double Scaba Anchor-Double PBTD Anchor-Double PBTU	Radial Down axial Up axial	Anchor-PBTU in the co-rotation mode led to better circulation of the gas phase.
[30]	Air-CMC (Power-law)	Coaxial	Anchor-A200 Anchor-A315 Anchor-A320	Down axial Down axial Down axial	Gas dispersion was intensified by increasing the solidity ratio of the central impeller.
[42]	Air-Xanthan Gum (Power-law)	Triple	RT HBT WHD WHU MIG	Radial Radial Down Axial Up Axial Axial	Triple RT exhibited the highest volumetric mass transfer coefficient
[100]	Air-Xanthan Gum (Power-law)	Double	RT EED EEU	Radial Down Axial Up Axial	The configuration EED-EEU provided adequate mass transfer coefficient, lower power consumption, and lower shear rate (desired for shear-sensitive cells).
[101]	Air-CMC (Power-law)	Coaxial	Anchor-Scaba Anchor-PBTU Anchor-PBTD Anchor-PBT/Rushton Anchor-PBT Updown Anchor-ASI Anchor- ASI Slanted Anchor-SJFEM	Radial Up axial Down axial Radial/Axial Up/Down axial Radial/Axial Up/Down axial Down axial	Helicity instabilities indicated poor aeration efficiency. Energy-efficient gas dispersion was achieved by the ASI impeller with negative helicity.

3.1. Single Impellers

The main challenge of gas-liquid mixing with non-Newtonian media is to promote homogeneous mixing for adequate mass transfer. This is because the mixing of shear-thinning fluids results in a well-mixed region close to the impeller blades and a poor-mixed region far from the impeller [90]. In this regard, close clearance impellers such as the helical ribbon have been investigated as an alternative to enhance the mixing performance and to avoid the formation of stagnant zones [102,103]. This impeller type provides a macromixing in the vessel, which contrasts with the local mixing promoted by high-speed central impellers. Wide-viscosity-range impeller type is an additional alternative to promote macromixing in fluids exhibiting complex rheology. This impeller configuration was investigated by Liu et al. [21], who employed a large-double-blade (LDB) impeller, a Fullzone (FZ) impeller, and a Maxblend (MB) impeller. They observed that the performance of each impeller type on the gas dispersion is highly affected by the rheological behavior of the fluid; FZ impeller promoted the best gas dispersion and mass transfer at low apparent viscosity, whereas MB impeller demonstrated better performance at higher apparent viscosity.

Nonetheless, Malik and Pakzad [15] mentioned that radial impellers have been traditionally employed due to adequate gas dispersion, representing over 80% of the gas-liquid mixing operations in industrial applications. In this regard, the correct assessment of the particularities of each mixing system with fluids that possess complex rheology is of main importance in order to choose a suitable impeller system [21]. For example, in mixing systems, including shear-sensitive cells, impeller types that induce a lower shear rate are often preferred, and the effect on the suspended cultures must be considered [104,105].

Khalili et al. [19] investigated the mixing time and relative power demand in a gas-liquid stirred vessel containing a yield stress fluid. They evaluated radial (Rushton turbine), axial (pitched blade turbine), and radial-axial (ASI) impellers. Even though the reduction in power uptake upon gassing when using ASI was not the smallest, this impeller type promoted the lowest mixing time. The radial impeller, in turn, promoted the highest power reduction but resulted in a lower mixing time compared to the axial impeller. Similarly, Malik and Pakzad [15] investigated the mixing time resulting from the gas dispersion in activated sludge (power-law fluid) using Rushton turbine, ASI (A200-Scaba), and ARI (A200-Rushton) impellers. Their results showed that the mixing time significantly depends on the impeller speed as well as on the interaction between impeller speed and gas flow number. Also, they reported that the lowest mixing time was obtained using the ASI impeller, similar to the outcomes reported by Khalili et al. [19].

For mixing performance in terms of the overall gas holdup in single impellers, Khalili et al. [20] showed that the Rushton impeller was slightly better than the ASI. Khare and Niranjan [106] investigated different radial impellers (bladed disk turbine, concave bladed disk turbine, and Scaba 6SRGT) for gas dispersion in highly viscous non-Newtonian fluids. They observed that, differently from Newtonian flows [107], the disk turbine demonstrated comparable or superior gas holdup than the other radial impellers. Also, Khare and Niranjan [106] reported that the agitation effect on the gas holdup depends on the fluid being evaluated and the aeration rate. For a CMC solution, the global gas holdup increased when increasing the impeller speed for all aeration rates. Differently, a non-monotonic effect of the impeller speed was observed for the gas holdup in polypropylene glycol containing CMC solution at low aeration rates, whereas the gas holdup monotonically decreases when increasing the impeller speed at a high aeration rate. For a xanthan gum solution, Liu et al. [21] reported that an increase in the impeller speed increased the gas holdup; however, this growth was reduced when increasing the xanthan gum concentration. This behavior indicates that a detailed investigation of the agitation effect is required for different fluid types in order to define optimum operating conditions to avoid unnecessary power consumption.

Khalili et al. [20] studied the agitation effect on the bubble diameter and observed that even though the impeller rotation affected the Sauter mean bubble diameter, it did not change the number of bubble classes in the mixing system. The bubble size distribution, in turn, depends on the cavity structure for a given impeller type, gas flow rate, and impeller speed, as presented by Momiroski et al. [65]. Their results also indicated that hollow blade turbines (HBT) generated smaller mean bubble sizes compared to Rushton turbines (RT). Furthermore, Cappello et al. [35] studied the agitation effect of a Rushton turbine on the bubble size and verified that an increase in power consumption due to the impeller rotation decreases the bubble mean diameter.

The effect of different single impeller types on the mass transfer coefficient was taken into consideration by Garcia-Ochoa and Gomez [108]. They compared the volumetric mass transfer coefficient in a stirred tank using different paddles and disk turbine impellers. The $k_L a$ increased when increasing the number of blades for both impeller types, and a better mass transfer effectiveness was observed for the disk turbine. Furthermore, several authors have verified that the volumetric mass transfer coefficient increases when increasing the agitation speed [40,95,109]. In fact, the mass transfer rate relies on the turbulent recirculation patterns, in which the small turbulent eddies break the bubbles and lead to a higher interfacial area between the phases [110]. However, Ogut and Hatch [111] observed that the

k_La is a weak function of the specific power consumption in the agitation of non-Newtonian fluids using a paddle-type impeller. Similarly, Tecante and Choplin [102] reported that the volumetric mass transfer coefficient increased more with increasing the aeration rate than increasing the impeller rotation speed, which implies that the mass transfer mechanism is mostly controlled by the aeration. It is worth noting that these results were closely related to the type of the impeller configuration employed in each study. The paddle-type impeller employed by Ogut and Hatch [111] was not suitable to increase the cavern size around the impeller, which directly affects the pumping capacity. In addition, Tecante and Choplin [102] employed a helical ribbon screw, which is a close-clearance impeller that applies low shear stress into the mixing systems. Therefore, it explains the more significant effect of the aeration on the k_La compared to the impeller rotational speed.

3.2. Multiple Impellers

Multiple impeller configurations are often employed to promote a more uniform bubble distribution compared to a single impeller configuration, especially when aspect ratios are larger than one [49,112]. Besides the superior performance for mass transfer, double impellers on the same shaft require less power compared to two single impellers separately, which suggests significant savings on an industrial scale gas purged mixing system [113]. When a low shear rate is required, a configuration of multiple close clearance impellers is suitable. This mixing configuration is also suitable for a better mixing performance of shear-thinning fluids [114]. However, it is important to note that some particularities for these impellers may appear. For example, Amiraftabi et al. [115] studied a gas-liquid dispersion system using a dual helical ribbon impeller and reported that an increase in impeller speed does not always reduce the mixing time. This indicates that an optimum rotational speed needs to be found.

Other multiple impeller configurations have been evaluated as reported in the literature. For instance, Cabaret et al. [88] studied double impellers in centered and off-centered positions, and the latter configuration had a negative effect on the mass transfer performance for shear-thinning fluids described by the power-law model. Valverde et al. [23] used computational simulation to evaluate the performance of centered double Rushton impellers for gas dispersion and mass transfer in a xanthan gum solution. They observed that both gas holdup and mass transfer coefficient increased when increasing the impeller speed and aeration rate. However, the gas holdup was more sensitive to the variation in the rotation speed.

Suhaili et al. [116] investigated the mass transfer performance in a gas-liquid mixing system with non-Newtonian media using different radial impellers in a dual impeller configuration. They observed that double concave-bladed disc turbines demonstrated better performance when compared to the double Rushton turbine configuration due to an enhanced gas handling. Gabelle et al. [22], on the other hand, evaluated different impeller types (Rushton turbine, PBT, and Mixel TT) in a dual impeller configuration and observed that the mass transfer was not affected by the stirrer design at a fixed power consumption. Instead, the tank size significantly influenced the mass transfer in most of the viscous fluids. Other six different stirrers in a triple impeller configuration were investigated by Xie et al. [42] for gas dispersion in xanthan gum solutions: 3RT, HBT+2WHD, HBT+2WHU, HBT+2MIG, EG, and HBT+DHR. They reported that a triple Rushton turbine (3RT) provided the highest average volumetric mass transfer coefficient, and a combination of a hollow blade turbine and a double helical ribbon (HBT+DHR) provided the lowest k_La. However, a high variation in mass transfer rate throughout the vessel can be observed when combining small-diameter impellers, whereas a more homogeneous distribution is observed for large-diameter impellers. In this regard, coaxial mixer is an alternative for enhancing the mixing performance because it combines the advantages of both impeller types (small-diameter and large-diameter impellers).

Coaxial Mixers

Although single shaft impellers are commonly employed in industrial processes due to their easy operation and well-known design methods, they are usually designed to meet the requirements of specific applications [117]. These systems, however, are prone to failure in rheologically evolving processes, and alternative configurations such as coaxial mixers should be employed to overcome such challenges.

Coaxial mixers employ two concentric, motor-driven shafts, in which high-speed impellers are combined with low-speed close-clearance impellers [118]. The close-clearance impeller enhances the homogenization by moving the fluid near the wall to the center of the vessel. The synergistic hydrodynamic effect of impellers rotating independently promotes an advantageous mixing performance for rheologically complex systems [119]. Regardless of the costs associated with the construction and maintenance of coaxial mixers, they promote good mixing characteristics in high viscous fluids and a more uniform spatial distribution of the shear rate [88,120].

A few studies have evaluated coaxial mixers for gas-liquid dispersion applications, and scant data is available for gas dispersion in non-Newtonian fluids. Espinosa-Solares et al. [121] studied a helical ribbon-Smith turbine coaxial mixer and reported a good gas dispersion in both Newtonian and non-Newtonian fluids based on visual observation. Also, shorter mixing times were reported compared to single impellers [122]. Jegatheeswaran et al. [30] analyzed coaxial mixers comprised of an anchor impeller and different axial inner impeller types (A200, A315, and A320) and reported a non-monotonic effect of the speed ratio on the local and global gas holdup. Later, Jegatheeswaran and Ein-Mozaffari [33] observed that high impeller speed did not contribute to enhancing the gas holdup throughout the vessel when using a Scaba-Anchor coaxial impeller. These results suggest that the hydrodynamics promoted by the central impellers significantly influences the gas dispersion.

The hydrodynamic effect of the central impeller was also investigated by Jamshidzadeh et al. [37]. They observed that using a double down-pumping pitched blade turbine generated a higher volumetric mass transfer coefficient than using a double up-pumping pitched blade turbine or double Scaba impellers. Similarly, Liu et al. [18] studied different single central impeller types and observed that even though PBT exhibited the highest mass transfer coefficient, the BDT-6 impeller exhibited a better gas pumping capacity. Jegatheeswaran and Ein-Mozaffari [101], in turn, reported that a radial-axial impeller named ASI was the most energy-efficient impeller in dispersing the gas compared to Scaba, PBT, ASI Slanted, PBT Updown, and PBT-Rushton impellers. With respect to the rotation mode, Liu et al. [123] utilized computational simulations and reported that counter-rotation mode promoted superior gas distribution, which was later considered by Liu et al. [18]. On the other hand, other authors reported superior mixing performance of co-rotation mode [29,49].

4. Aeration Effect

Several studies have addressed the aeration effect on different mixing and mass transfer variables. For example, Ogut and Hatch [111] showed that the gas flow rate significantly affects the volumetric mass transfer coefficient. From their results, the aeration had a direct effect on the volumetric mass transfer coefficient, which was also reported by other authors [18,21,37,108]. In this regard, the aeration increases the number of bubbles inside the vessel that leads to an increase in the mass transfer rate [40]. In fact, the aeration effect on $k_L a$ can be even more significant than the agitation effect in certain impellers, such as the helical ribbon screw [102]. However, the combination between aeration and agitation phenomena determines which variable controls the mass transfer. For instance, the stirrer agitation has a more significant influence at low aeration rate, whereas the mass transfer is controlled by the aeration at high gas flow rate [37].

Cascaval et al. [124] showed that in bioreactors systems that require gas dispersion in broths, the aeration increased the mass transfer rate due to an increase in the oxygen concentration gradient between the phases. This effect was observed for model fluids, bacterial, and yeast broths. However, an increase in the aeration rate promoted a non-

monotonic behavior on the mass transfer coefficient for fungal broths, in which the k_La reached a minimum value when increasing the gas flow rate.

Similar to the volumetric mass transfer coefficient, the gas holdup is directly influenced by the aeration rate [20,21,110]. However, the rate of increase in gas holdup is reduced as the gas flow rate increases, which means that there exists an upper limit for aeration, such that an undesired flooding condition occurs above this aeration limit. A comprehensive knowledge of the system is required to enable increasing the aeration while keeping the flow regime under full dispersion or loading regime. It is worth noting that due to the complex phenomena that encompass the gas-liquid mixing, especially with non-Newtonian fluids, different gas holdup patterns may be observed when varying impeller speed at different air flow rates, as observed by Jamshidzadeh et al. [49] for coaxial mixers.

It is well-known that the power consumption in mixing vessels decreases upon aeration due to the formation of cavities behind the blades that can reduce the rotational resistance of the stirrer [19,22,125]. The reduction rate in power consumption, however, becomes smaller as the gas flow rate increases [18]. In non-Newtonian fluids, these cavities tend to be more stable, which promotes a higher decrease in power uptake [18]. Nevertheless, the mixing power is not significantly affected by the aeration rate at low Reynolds numbers, since its effect is also dependent on the flow regime [125]. In addition to that, an increase in the aeration rate increases the minimum impeller speed required for complete dispersion [19].

Moreover, Khalili et al. [20] showed that the variation in gas flow rate did not vary the number of bubble classes observed in a mixing system, even though the Sauter mean diameter increased when increasing the aeration rate. An increase in the bubble mean size upon gassing was also observed by Cappello et al. [35]. Higher aeration favors the bubble coalescence and reduces the energy transferred by the stirrer, which are the main reasons for bigger Sauter mean diameters [35,110]. As the bubble diameter increases, the residence time of these larger bubbles decreases, which explains the reduction in the rate of increase in gas holdup when increasing the aeration rate [18].

The mixing time is also influenced by the gas flow rate. In general, the aeration enhances the axial mixing, which decreases the mixing time [15,115]. This is corroborated by an increase in the fraction of well-mixed zone when increasing the gas superficial velocity, which was observed by Triveni et al. [31]. However, the aeration effect on the mixing time also depends on the flow regime in the vessel [120,122]. For example, the mixing time increases during the onset of dispersion. In this regard, attention is necessary when increasing the gas flow rate aiming at achieving minimum mixing time because it can lead to the flooding regime, which is not desired [122]. It is also worth noting that although the upward gas flow can enhance the axial bulk mixing, it has only a small effect on the average shear rate, as shown by Campesi et al. [126].

Regarding the sparger type, several studies have evaluated this effect on the mixing and mass transfer characteristics. Garcia-Ochoa and Gomes [108] reported that the type of gas supply did not significantly affect the mass transfer rate. On the other hand, Liu et al. [127] demonstrated that a micro-orifice gas distributor enhanced the gas-liquid mixing performance in a xanthan gum solution compared to a traditional ring sparger. The micro-orifice sparger reduced the bubble size injected into the vessel and led to a higher residence time, augmented gas holdup, and enhanced interfacial area, which increased the mass transfer rate.

5. Rheological Effect

The rheological effect on gas-liquid mixing systems has been mainly studied by considering the apparent viscosity value. The apparent viscosity is defined as the ratio between shear stress and the shear rate. At first, it is important to notice that it is not straightforward to obtain the viscosity experimentally, since it changes with the shear rate for non-Newtonian fluids. In fact, the measurement of local shear rate is not simple [128]. Hence, some empirical correlations are available in the literature to obtain the average

shear rate, as presented in Table 6. The correlation proposed by Metzner and Otto [129], however, is well-established and is widely applied in many works [21,35,40,88]. Although this correlation originally assumes a laminar flow regime, it can also be applied in turbulent regime [130].

Table 6. Empirical correlations to predict average shear rate.

Correlation	Mixing System	Reference
$\dot{\gamma}_{av} = K_i N^{3/(1+n)}$	Shear-thinning fluids in turbulent regime	[126]
$\dot{\gamma}_{av} = \left(\frac{a}{d}\right)^{\frac{1}{c(1-n)}} k^{\frac{c-f}{c(1-n)}} N^{\frac{b-e}{c(1-n)}}$		[128]
$\dot{\gamma}_{av} = K_s N$	Shear-thinning fluids in laminar regime	[129]
$\dot{\gamma}_{av} = K_s \left(\frac{4n}{3n+1}\right)^{\frac{n}{n-1}} N$		[131]

Several authors have observed that the volumetric mass transfer coefficient is inversely affected by the apparent viscosity of non-Newtonian fluids [13,18,40,108,110,111]. Overall, a decrease in volumetric mass transfer coefficient upon increasing the apparent viscosity of the fluid is a result of the decrease in the size of the well-mixed region [31]. Ranade and Ulbrecht [110] observed that a steeper decrease in the mass transfer coefficient can be obtained for pseudoplastic fluids with viscoelasticity, compared to a pseudoplastic fluid without viscoelasticity. This is explained by the increase of the elongation viscosity, which allows the bubbles to deform instead of breaking up. Park et al. [132] further evaluated the effect of the elastic properties of the fluids and included the dimensionless Deborah number in the $k_L a$ empirical correlation. Their results corroborated that the elastic effects reduce the volumetric mass transfer coefficient. Gomez-Diaz and Navaza [40] emphasized the importance of considering the rheological effects on the mass transfer characteristics in mixing systems. They observed that the $k_L a$ was highly affected by the composition of two polymers in a liquid solution: carboxymethyl cellulose (CMC) and alginate (ALG). The variation in the composition varied the rheological parameters, which affected the mass transfer coefficient in different ways, depending on the combination of process conditions.

It is known that an increase in the apparent viscosity, as a result of an increase in the polymer concentration, decreases the dispersion capability [109]. This effect can lead to reducing the global gas holdup as demonstrated by Machon et al. [51] for pseudoplastic fluids. They observed that the overall gas holdup decreases when the polymer concentrations are high enough to promote the formation of large bubbles, which decreases the residence time due to higher bubble rise velocity. However, the effect of the physical properties on the gas distribution is complex. Vlaev et al. [133] studied the effects of the apparent viscosity on the local gas holdup and their results showed that an increase in polymer concentration increased the resistance to the rise of small bubbles near the vessel wall, whereas a better gas circulation can be observed in the region close to the impeller due to higher shear rate. Liu et al. [18] and Ali and Solsvik [110] reported that the gas holdup increased for higher polymer concentration (i.e., higher apparent viscosity), which was a result of the resistance to bubble rise in their case.

Nienow et al. [90] studied the power consumption for gas dispersion in rheologically complex fluids that included viscoelastic effects and yield stress. For yield stress fluids, they observed the formation of cavities upon aeration, which remained present in the vessel even when the gas was switched off. This phenomenon is known to reduce the relative power demand since the cavities reduce the dispersion capability. Similarly, Liu et al. [18] showed that the relative power demand decreases when increasing the xanthan gum concentration.

Even though several studies have shown that fluid rheology significantly affects mixing and mass transfer characteristics, an understanding of these phenomena is still not completely recognized. Further studies are required to enlighten how individual parameters, such as apparent viscosity, consistency, degree of pseudoplasticity, and yield stress, affect the gas-liquid mixing behavior. In fact, the investigation of the hydrodynamics of these mixing systems allows addressing the aeration and agitation phenomena for

various rheologically complex fluids. The overall performance of mechanically agitated vessels to disperse gas in non-Newtonian fluids is summarized in the diagram presented in Figure 4.

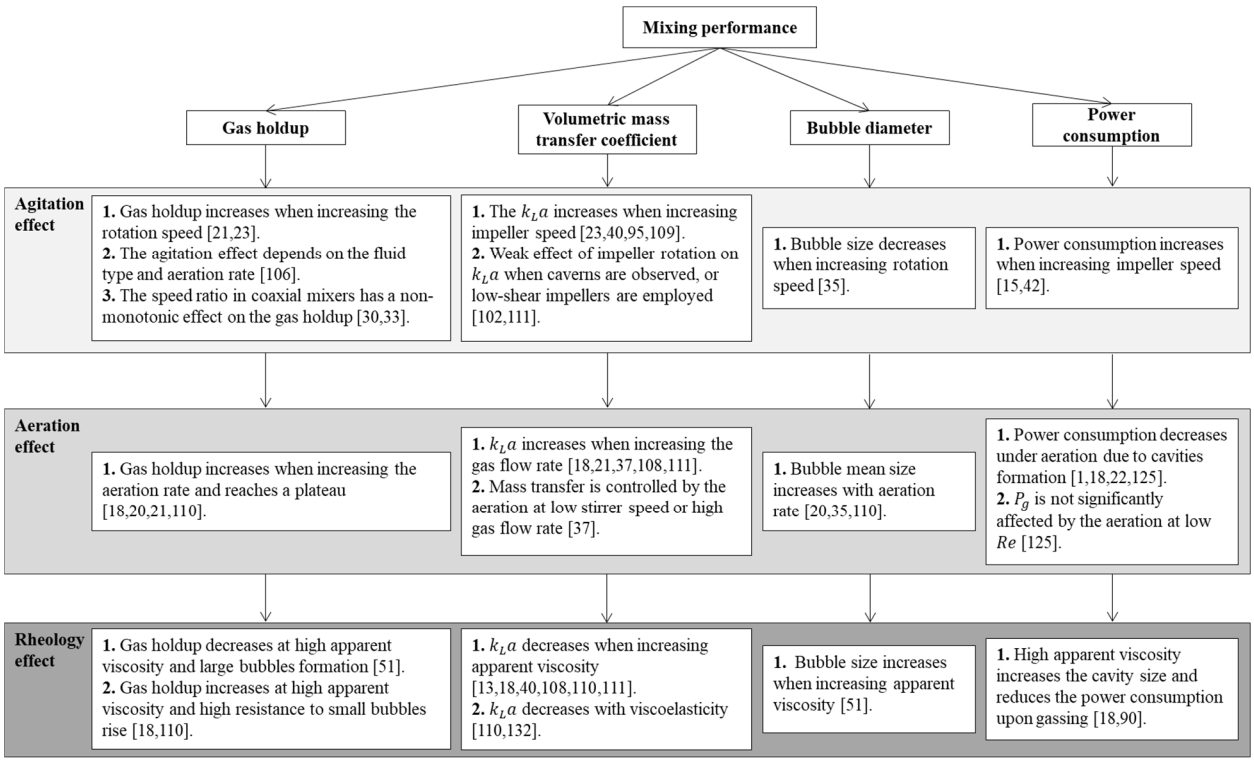

Figure 4. Summary of overall gas-liquid mixing performance using mechanically agitated vessels with non-Newtonian fluids.

6. Computational Fluid Dynamics

Computational Fluid Dynamics (CFD) has been widely employed for mechanically agitated vessels' simulations to obtain a detailed description of the fluid flow behavior. This analysis enables to accurately verify local variables throughout the vessel, such as gas holdup, volumetric mass transfer coefficient, and velocity of each phase [134]. Also, it provides information about variables that cannot be measured experimentally, such as the local shear rate and local viscosity values of non-Newtonian liquids throughout the vessel. A wider understanding of the flow pattern for these mixing vessels with complex fluid is essential to enlighten the effect of operating and design parameters on the mixing and mass transfer characteristics, especially in those cases where the fluid is opaque. In addition to this, experiments are more costly compared to numerical analyses; thus, numerical simulations are often considered a convenient and helpful tool in evaluating such complex gas-liquid hydrodynamics [135–137].

It is worth mentioning that the CFD simulations need to be validated using experimental data because of the assumptions and closure models [7]. The accuracy of the model for lab-scale gas-liquid mixing systems is often evaluated in terms of the measured gas holdup and power consumption [16,29,33]. Once it is validated using the experimental data, other process conditions and design parameters can be simulated. For instance, the validated CFD model can be utilized for the scale-up because the models are based on fundamental physics and are scale-independent. In fact, the CFD models of the pilot-scale and industrial-scale can be developed and simulated just as easily as the lab-scale model. Table 7 shows different configurations of agitated vessels that have been investigated using CFD and highlights some numerical approaches taken into consideration in each study.

Table 7. CFD simulations of agitated vessels for gas dispersion in non-Newtonian fluids.

Reference	Fluids	Impeller Configuration	Tank Size (m^3)	Flow Regime	Drag Model	Bubble Size	Rotation Approach	Software
[16]	Air-XG solution (Power law model)	Six-blade Rushton Turbine	0.02, 22, and 100	Turbulent ($k-\varepsilon$ model)	Scargiali et al. [138]	Constant (experimentally measured between 3.4 and 6 mm)	SM and MRF	Fluent 2019 R2
[19]	Air-XG solution (Herschel-Bulkley model)	PBT; ASI; Rushton disk turbine	0.05	Laminar	Schiller-Naumann model	Constant (2.5 mm)	SM	Fluent 16.1
[23]	Air-XG solution (Power law model)	Dual Rushton turbine	0.004	Turbulent (SST and $k-\varepsilon$ model)	Schiller-Naumann model	Constant (2, 3, and 4 mm)	MRF	Fluent 14.5
[29,32,49]	Air-CMC solution (power law model)	Double Scaba-Anchor; Double PBT-Anchor	0.0628	Laminar	Schiller-Naumann model	Size Distribution (3–10 mm)	SM	Fluent 19
[30]	Air-CMC solution (Power law model)	A200-Anchor; A315-Anchor; A320-Anchor	0.05	Laminar	Schiller-Naumann model	Constant (2.5 mm)	SM	Fluent 16.2
[33]	Air-CMC solution (Power law model)	Scaba-Anchor	0.05	Laminar	Schiller-Naumann model	Size Distribution (2.5–10 mm)	SM	Fluent 16.2
[38]	Air-XG solution (Carreau *model*)	Dual Rushton turbine	0.2 and 70	Turbulent (SST and $k-\varepsilon$ model)	Tzounakos et al. [139]	Constant (4 and 5 mm)	MRF	CFX 5.7
[140]	Air-NaCMC (Power law model)	Dual helical ribbon	0.01	Turbulent ($k-\varepsilon$ model)	Schiller-Naumann model	Population balance model (0.1–7 mm)	MRF	Fluent R19.1

Setting accurate bubble size characteristics is crucial to obtain numerical results close to experimental data. This is directly related to the drag model, and consequently, entirely affects the hydrodynamics of the gas-liquid mixing. Also, the flow regime needs to be set by taking into consideration the previous knowledge of the system, such as the physical properties of the fluids. For example, a system containing a yield-stress fluid modeled by the Herschel-Bulkley model is normally simulated using a laminar flow regime. Regarding the modeling of the impeller rotation, the CPU time is an important factor to determine if the multiple reference frame (MRF) should be employed instead of the sliding mesh (SM) technique. Sliding mesh is a transient approach and usually predicts the fluid flow with the best agreement against experimental data, requiring a higher computational effort. Nevertheless, the prediction of global hydrodynamics variables is not significantly sensitive to the approach employed for the modeling of the impeller rotation, so that MRF is more computationally efficient as reported by Cappello et al. [16].

7. Gas Dispersion in Yield-Stress Fluids with Coaxial Mixers

From the literature review discussed in previous sections, a knowledge gap was identified for gas dispersion in pseudoplastic fluids with yield stress. These fluids are commonly employed in pharmaceutical, food, and chemical processes [11]. Therefore, the investigation of energy-efficient mixing configurations is highly desirable for these applications. Coaxial mixers, in turn, have demonstrated advantageous features for dispersing gas in pseudoplastic fluids and for the mixing of single-phase yield stress fluids [28,29,33]. However, their applicability to gas dispersion in yield stress fluid is still uncertain. In view of that, this work compared the mixing performance of a coaxial mixer (Anchor-PBU) against a single impeller configuration (fixed anchor, N_A= 0 rpm) for gas dispersion in the xanthan gum solution (1 wt%) with a constant gas flow rate of 10 L/min. Four central

impeller speeds were tested (190, 310, 430, and 550 rpm), and the anchor impeller speed was set at 10 rpm in the co-rotation mode for the coaxial mixer configuration.

Electrical resistance tomography (ERT) was used to measure the gas holdup, and computational fluid dynamics (CFD) modeling was used to predict the flow pattern within the vessel. The rheological behavior of the xanthan gum was obtained experimentally via the Bohlin CVOR Rheometer 150 (Malvern Instruments, USA), and the parameters for the Herschel-Bulkley model were estimated as shown in Equation (6):

$$\tau = 3.852 + 1.637\dot{\gamma}^{0.370} \tag{6}$$

The stirred vessel, with a diameter of 40 cm, had a fluid volume of 0.05 m^3. The dimensions of the tank and anchor were the same as previously studied by Jegatheeswaran and Ein-Mozaffari [28]. However, a pumping-upward pitched blade turbine (PBT) was employed instead of the Scaba impeller. Detailed information about the impellers dimensions is given in Table 8. Moreover, the schematic diagram in Figure 5 illustrates the ERT method used to measure the gas holdup based on the conductivity of the fluid inside the vessel.

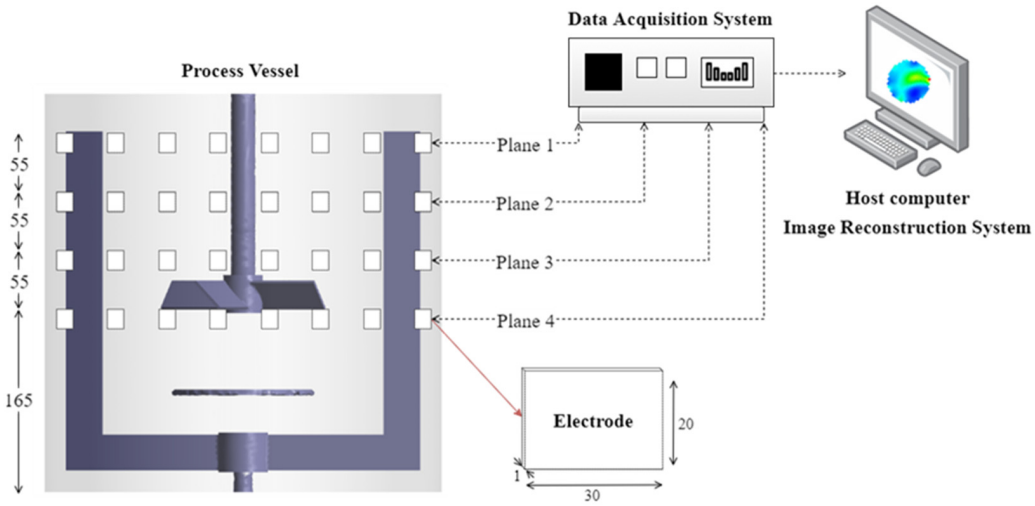

Figure 5. Schematic diagram of electrical resistance tomography technique.

Table 8. Dimensions of the impellers utilized in the coaxial mixer.

Dimensions	Value (mm)	
	Anchor	PBT
Diameter	360	180
Height	360	38
Width	36	70
Thickness	10	4
Clearance	20	180
Impeller hub diameter	50	40
Impeller shaft diameter	20	25

The experimental results for the global gas holdup are shown in Figure 6. The use of single impeller configuration ($N_A = 0$ rpm) resulted in less efficient mixing, which is even more apparent for lower central impeller speeds. At 550 rpm, however, the mixing performance of the two configurations was approximately the same. It indicates that the single impeller requires a higher impeller rotation to result in a global gas holdup close to the coaxial mixer. In fact, this demonstrates the superior performance of the coaxial mixer compared to that of a single impeller because it reaches a higher gas holdup at lower central

impeller speeds, which is particularly advantageous for systems with non-Newtonian fluids.

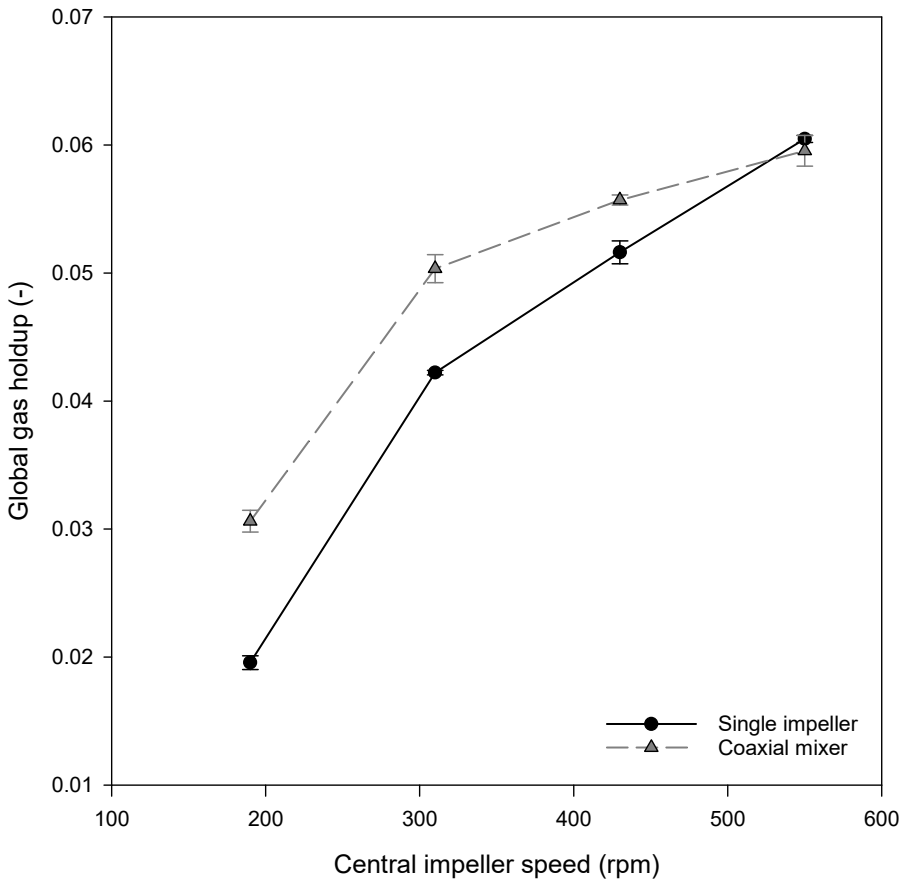

Figure 6. Gas holdup at different central impeller speeds for a single impeller and a coaxial mixer.

Fluent 2020 R1 was utilized to simulate the mixing system aiming at having a better insight into the fluid flow throughout the vessel. The Eulerian-Eulerian multiphase approach was employed, such that both continuous (xanthan gum solution) and dispersed (air bubbles) phases are considered fully interpenetrating. The dispersed phase was defined with a constant diameter of 6 mm, and no mass transfer was considered. As reviewed in Table 7, virtual mass and lift forces were neglected and only the interphase momentum transfer due to the drag force was considered. The Schiller-Naumann model was employed to calculate the drag coefficient. In addition, the laminar flow regime was considered, and the sliding mesh approach was used to predict the impellers' rotation.

For the interpolation scheme, a second-order upwind was set for the momentum resolution and QUICK for the volume fraction. The SIMPLE algorithm was employed for pressure-velocity coupling, and a residual target of 1×10^{-7} was defined for the global root mean square (RMS). Furthermore, the boundary conditions were defined as presented in Table 9. It is worth noting that the model was validated against experimental gas holdup so that the fluid flow can be evaluated in detail, knowing that it truly represents the actual mixing phenomenon.

In terms of flow patterns, the main objective of mixing processes is to create well-defined mixing zones. From Figure 7, it can be observed that the single impeller configuration did not create the proper circulation loops. On the other hand, the synergetic agitation of the co-rotation configuration resulted in well-defined circulation loops close to the impellers and minor circulation loops near the tip of the anchor impeller in the coaxial mixer.

Table 9. Boundary conditions for the CFD simulation.

Location	Boundary Condition
Sparger holes	Inlet: The mass flow rate of air was specified at this boundary
Impeller walls	Moving wall: The rotation speed was specified as the same as the adjacent rotating zone
Vessel wall	Stationary wall: Non-slip condition
Liquid surface	Outlet: No air backflow was allowed

These results corroborate the mixing performance in terms of gas holdup and indicate an enhanced gas dispersion in yield stress fluid when using a coaxial mixer compared to a single impeller. However, future investigation is still required to analyze the effect of each impeller speed and gas flow rate on the bubbles dispersion.

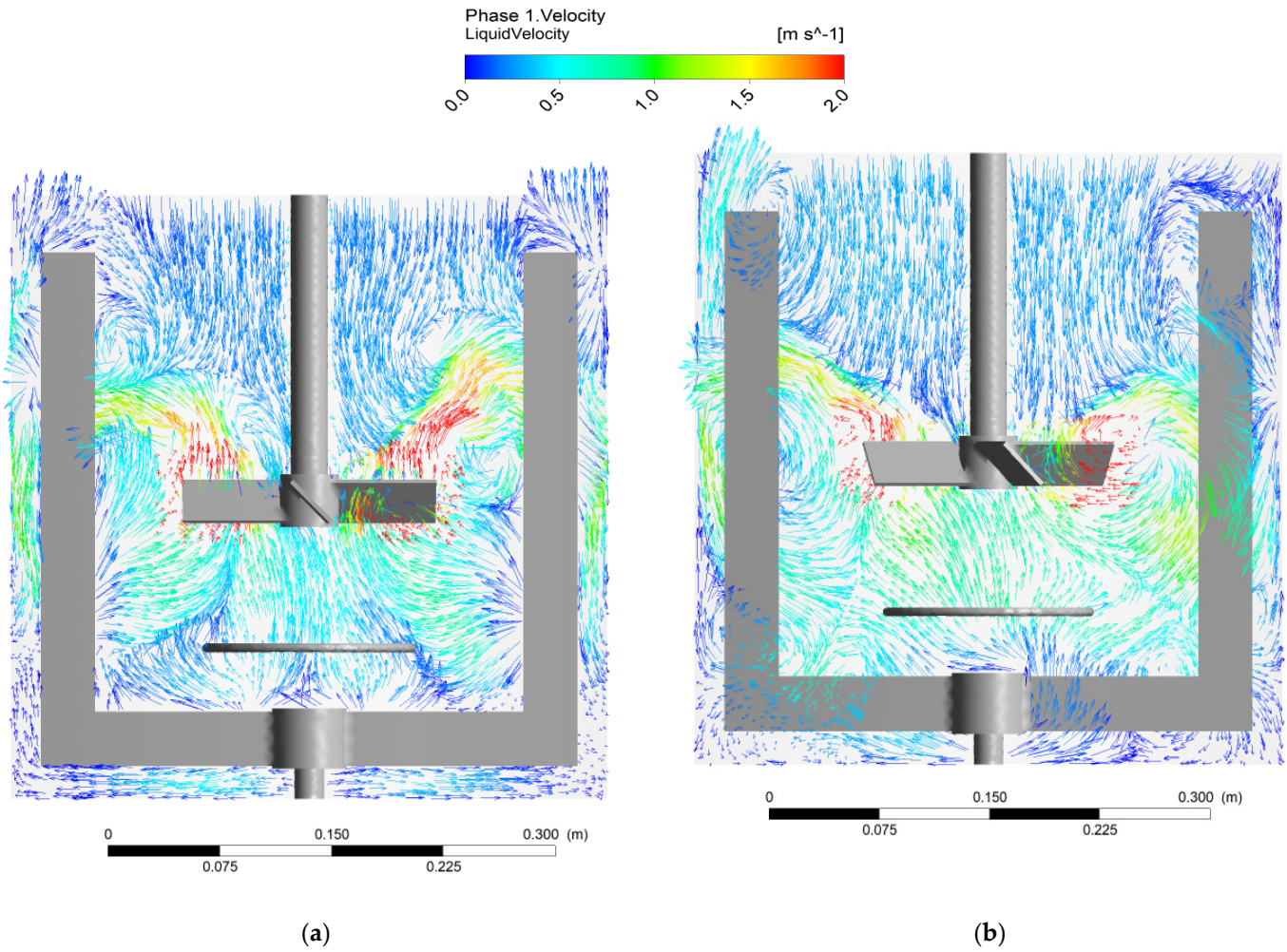

(**a**) (**b**)

Figure 7. Flow patterns for (**a**) single impeller (fixed anchor), and (**b**) coaxial mixer.

8. Scale-Up

The scale-up of mechanically agitated vessels aims to design large-scale systems with equal mixing quality compared to that in the laboratory or pilot scale [6]. This is a complex task and encompasses different scale-up strategies. The rule of thumb is the most common approach, which is based on empirical estimations and experience; hence, it is limited by the range of applicability of the empirical correlations [53]. Since it is impossible to keep all mixing parameters constant when scaling-up the mixing system, it is necessary to evaluate critical factors for specific applications and priorities have to be selected [6].

Among the scale-up criteria used as a rule of thumb, the following may apply: geometric similarity, equal specific power consumption, equal impeller tip speed, constant mixing time, and equal volumetric mass transfer coefficient [141]. In addition, a combination of design variables may also apply as a scale-up criterion. Nevertheless, the main concern of scale-up using the rule of thumb is related to the applicability of empirical correlations obtained from small-scale equipment [142]. The flow regime in small-scale devices is often kept as homogeneous; however, industrial-size systems normally exhibit a heterogeneous flow regime such that the available correlations may not be adequately applicable [143].

A wide industrial applicability of gas dispersion in non-Newtonian systems can be observed in bioreactions, such as in antibiotics production, fungal fermentation, and cell culture. Bioreactors generally require a good supply of oxygen to the media; therefore, the mass transfer variables are normally the main scale-up factors [18,144]. One of the challenges to maintain a certain mass transfer level during the scale-up of these processes is the complex rheology of the non-Newtonian fluids [145]. The spatial heterogeneity due to the viscosity variation is sensitive to the equipment size, which directly affects the degree of contact between the phases [31,111]. Also, additional challenges are related to geometric similarity. Normally, industrial-size bioreactors employ multiple impellers whereas a bench-scale system uses a single impeller, meaning that the geometric similarity is not maintained [145].

Some examples of the scale-up of bioreactors are detailed in the literature. For instance, Qu et al. [144] investigated a fed-batch fermentation process of docosahexaenoic acid (DHA) production by Schizochytrium sp. and studied a scale-up strategy that kept the volumetric mass transfer coefficient constant. They achieved a successful performance for a maximum volume scale-up factor of 1:150, obtaining similar k_La values for shake flasks, bench-scale, and pilot-scale. Hardy et al. [145] evaluated three different scale-up criteria for *Trichoderma reesei* batch culture: tip speed velocity, specific power drawn, and energy dissipation/circulation function (EDCF). Their analysis indicated the EDCF criterion as the best one to overcome the complexities in bioreactors containing non-Newtonian fluids.

Gabelle et al. [22] investigated different scale-up parameters for gas dispersion in shear-thinning fluids that can be used as model fluids for biological suspensions. They proposed empirical correlations to predict the relative power demand and mass transfer coefficient for different scales (42 and 340 L vessels). The relative power demand was predicted with an accuracy of approximately 10%, whereas the accuracy of the volumetric mass transfer coefficient correlation was approximately 20%. Computational fluid dynamics simulations can also be used to analyze the effect of the vessel size on the design variables [16]. In fact, the comprehensive analysis of the hydrodynamic behavior throughout the vessel in different scales is highly desired to have a better understanding of the fluid flow upon scaling-up. However, there are some numerical limitations in simulating commercial-scale equipment because it requires a high number of mesh elements that lead to a high computational effort [146]. Normally, model simplifications are needed in these cases but still a good prediction of the fluid behavior can be obtained from CFD analyses.

9. Final Considerations

This work presented a comprehensive review of the effect of agitation, aeration, and rheological properties on the gas dispersion in non-Newtonian fluids. The mixing performance variables, such as the gas holdup, power consumption, bubble size, and volumetric mass transfer coefficient, were discussed by introducing the main existing experimental techniques and empirical correlations. The empirical correlations suggested by previous researchers are the most straightforward way for evaluating the effect of operating and design parameters on the mixing performance variables. However, the correlations are limited to specific ranges of fluid properties, impeller configuration, and process conditions.

In addition, this review paper discussed the individual influence of impeller design, configuration, rotation speed, gas flow rate, and rheological properties on the power

consumption, gas holdup, and mass transfer coefficient, based on recent investigations available in the literature. The studies show that the mixing and mass-transfer characteristics in aerated vessels containing non-Newtonian fluids significantly vary with operating conditions. It means that each specific process condition must be evaluated in detail to avoid misleading conclusions about this complex fluid flow. In fact, a complete understanding of the gas-liquid mixing processes containing non-Newtonian fluids is far to become clear. This is due to the vast range of rheological properties that can be obtained, which significantly affect the flow behavior and, therefore, the mixing and mass transfer phenomena.

Future studies providing additional experimental measurements of mixing and mass transfer variables in aerated stirred vessels are highly desired. For instance, there is a lack of experimental data for gas dispersion in yield stress fluids and viscoelastic fluids. This paper also presented the preliminary results for the gas dispersion in the yield-pseudoplastic fluids with coaxial mixers. These data revealed that the coaxial mixers are more energy-efficient compared to a single impeller. The coaxial mixer (Anchor-PBU) resulted in a higher gas holdup which was explained by the flow patterns predicted by the CFD model. Moreover, different vessel scales, impeller designs, and impeller configurations still need to be investigated for better comparative analyses. In these cases, local mixing performance variables should be preferably measured in order to assess the degree of homogeneity in the stirred vessel. In addition to the experimental data, numerical investigation from computational fluid dynamics also provides valuable information for the design of gas-liquid mixing vessels with non-Newtonian fluids, such as the shear rate and viscosity variation throughout the vessel. In fact, these numerical simulations are essential to comprehend the gas dispersion phenomenon in complex fluids since the system performance essentially depends on the fluid flow behavior. Both experimental and numerical approaches can also be applied to shed light on the scale-up of stirred vessels utilized for gas dispersion in non-Newtonian fluids. These analyses allow us to propose an adequate scale-up strategy aiming at maintaining a specific variable constant, such as the volumetric mass transfer coefficient, and enable us to verify the trade-offs of the scale-up approach for the industrial-scale mixing performance.

Author Contributions: P.L.B.: Conceptualization, Methodology, Software, Validation, Formal analysis, Writing—original draft. F.E.-M.: Conceptualization, Resources, Methodology, Writing—review & editing, Supervision, Project administration, Funding acquisition. A.L.: Conceptualization, Resources, Methodology, Writing—review & editing, Supervision, Project administration, Funding acquisition. All authors have read and agreed to the published version of the manuscript.

Funding: This research was funded by Natural Sciences and Engineering Research Council of Canada grant number RGPIN-2019-04644.

Institutional Review Board Statement: Not applicable.

Informed Consent Statement: Not applicable.

Data Availability Statement: Not applicable.

Acknowledgments: The financial support of the Natural Sciences and Engineering Research Council of Canada (NSERC) is gratefully acknowledged.

Conflicts of Interest: The authors declare no conflict of interest.

Nomenclature

d_{32}	Sauter mean bubble diameter	m
d_b	Bubble diameter	m
D	Impeller diameter	m
D_c	Central impeller diameter	m
f_{Pa}	Anchor power fraction	−
f_{Pc}	Central impellers power fraction	−
Fl	Gas flow number	−

Fr	Froud number	–
g	Gravitational acceleration	m s^{-2}
k	Consistency index	Pa s
k_La	Volumetric mass transfer coefficient	s^{-1}
K_s	Metzner and Otto constant	–
M	Torque	N m
M_A	Anchor torque	N m
M_C	Central impeller torque	N m
n	Power-law index	–
N	Impeller speed	s^{-1}
N_A	Anchor impeller speed	s^{-1}
N_C	Central impeller speed	s^{-1}
N_{cd}	Impeller speed for complete dispersion	s^{-1}
N_f	Impeller speed for flooding regime	s^{-1}
N_R	Speed ratio	–
P_g	Gassed power	W
P_o	Power number	–
P_u	Ungassed power	W
Q	Gas flow rate	m^3 s^{-1}
r	Cavern radius	m
Re	Reynolds number	–
R_N	Speed ratio	–
T	Vessel diameter	m
V	Liquid volume	m^3
v_s	Superficial gas velocity	m s^{-1}
vvm	Volume of gas per volume of liquid per minute	min^{-1}
X_{xg}	Mass concentration of xanthan gum	wt%
X_{cmc}	Mass concentration of CMC	wt%
We	Weber number	–
Greek Letters		
$\dot{\gamma}_{av}$	Average shear rate	s^{-1}
ε_g	Gas holdup	–
μ_c	Critical viscosity	Pa s
μ_L	Liquid viscosity	Pa s
μ_g	Gas viscosity	Pa s
μ_{ap}	Apparent viscosity	Pa s
ρ_L	Liquid density	kg m^{-3}
σ	Surface tension	N m^{-1}
τ_y	Yield stress	N m^{-2}
Acronyms		
ARI	A200/Rushton impeller	
ASI	A200/Scaba impeller	
BDT-6	Six curved-blade disc turbine	
CFD	Computational fluid dynamics	
CMC	Carboxymethyl cellulose	
DHR	Double helical ribbon	
EE	Elephant ear impeller	
EED	Elephant ear impeller pumping downward	
EEU	Elephant ear impeller pumping upward	
EG	Ellipse gate impeller	
HBT	Hollow blade turbine	
MRF	Multiple reference frame	
WHD	Wide-blade hydrofoil impeller pumping downward	
WHU	Wide-blade hydrofoil impeller pumping upward	
PBT	Pitched blade turbine	
PBTD	Pitched blade turbine pumping downward	
RT	Rushton turbine	
SM	Sliding mesh	

References

1. Leporini, M.; Terenzi, A.; Marchetti, B.; Corvaro, F.; Polonara, F. On the numerical simulation of sand transport in liquid and multiphase pipelines. *J. Pet. Sci. Eng.* **2019**, *175*, 519–525. [CrossRef]
2. D'Alessandro, V.; Giacchetta, G.; Leporini, M.; Marchetti, B.; Terenzi, A. Modelling blowdown of pressure vessels containing two-phase hydrocarbons mixtures with the partial phase equilibrium approach. *Chem. Eng. Sci.* **2015**, *126*, 719–729. [CrossRef]
3. Silva, C.R.; Esperança, M.N.; Cruz, A.J.G.; Moura, L.F.; Badino, A.C. Stripping of ethanol with CO_2 in bubble columns: Effects of operating conditions and modeling. *Chem. Eng. Res. Des.* **2015**, *102*, 150–160. [CrossRef]
4. Osadolor, O.A.; Jabbari, M.; Nair, R.B.; Lennartsson, P.R.; Taherzadeh, M.J. Effect of media rheology and bioreactor hydrodynamics on filamentous fungi fermentation of lignocellulosic and starch-based substrates under pseudoplastic flow conditions. *Bioresour. Technol.* **2018**, *263*, 250–257. [CrossRef] [PubMed]
5. Sluyter, G.; Kleber, J.; Perz, F.; Grund, B.; Leuchs, S.; Sieberz, S.; Bubenheim, P.; Thum, O. Fermentative oxidation of butane in bubble column reactors. *Biochem. Eng. J.* **2020**, *155*, 107486. [CrossRef]
6. Paul, E.L.; Atiemo-Obeng, V.A.; Kresta, S.M. *Handbook of Industrial Mixing: Science and Practice*; John Wiley & Sons, Inc.: Hoboken, NJ, USA, 2004.
7. Lee, B.W.; Dudukovic, M.P. Determination of flow regime and gas holdup in gas–liquid stirred tanks. *Chem. Eng. Sci.* **2014**, *109*, 264–275. [CrossRef]
8. Bao, Y.; Yang, J.; Wang, B.; Gao, Z. Influence of impeller diameter on local gas dispersion properties in a sparged multi-impeller stirred tank. *Chin. J. Chem. Eng.* **2015**, *23*, 615–622. [CrossRef]
9. Labík, L.; Moucha, T.; Petrícek, R.; Rejil, J.F.; Valenz, L.; Haidl, J. Volumetric mass transfer coefficient in viscous liquid in mechanically agitated fermenters: Measurement and correlation. *Chem. Eng. Sci.* **2017**, *170*, 451–463. [CrossRef]
10. Jamshed, A.; Cooke, M.; Ren, Z.; Rodgers, T.L. Gas–liquid mixing in dual agitated vessels in the heterogeneous regime. *Chem. Eng. Res. Des.* **2018**, *133*, 55–69. [CrossRef]
11. Marquez-Banos, V.E.; De La Concha-Gomez, A.D.; Valencia-Lopez, J.J.; Lopez-Yanez, A.; Ramirez-Munoz, J. Shear rate and direct numerical calculation of the Metzner-Otto constant for a pitched blade turbine. *J. Food Eng.* **2019**, *257*, 10–18. [CrossRef]
12. Chhabra, R.P.; Richardson, J.F. *Non-Newtonian Flow and Applied Rheology—Engineering Applications*, 2nd ed.; Elsevier: Amsterdam, The Netherlands, 2008.
13. Gabelle, J.-C.; Jourdier, E.; Licht, R.B.; Chaabane, F.B.; Henaut, I.; Morchain, J.; Augier, F. Impact of rheology on the mass transfer coefficient during the growth phase of *Trichoderma reesei* in stirred bioreactors. *Chem. Eng. Sci.* **2012**, *75*, 408–417. [CrossRef]
14. Garcia-Ochoa, F.; Gomez, E.; Alcon, A.; Santos, V.E. The effect of hydrodynamic stress on the growth of Xanthomonas campestris cultures in a stirred and sparged tank bioreactor. *Bioprocess Biosyst. Eng.* **2013**, *36*, 911–925. [CrossRef] [PubMed]
15. Malik, D.; Pakzad, L. Experimental investigation on an aerated mixing vessel through electrical resistance tomography (ERT) and response surface methodology (RSM). *Chem. Eng. Res. Des.* **2018**, *129*, 327–343. [CrossRef]
16. Cappello, V.; Plais, C.; Vial, C.; Augier, F. Scale-up of aerated bioreactors: CFD validation and application to the enzyme production by *Trichoderma reesei*. *Chem. Eng. Sci.* **2021**, *229*, 116033. [CrossRef]
17. Patel, D.; Ein-Mozaffari, D.; Mehrvar, M. Using Tomography to Characterize the Mixing of Non-Newtonian Fluids with a Maxblend Impeller. *Chem. Eng. Technol.* **2013**, *36*, 687–695. [CrossRef]
18. Liu, B.; Zheng, Y.; Cheng, R.; Xu, Z.; Wang, M.; Jin, Z. Experimental study on gas-liquid dispersion and mass transfer in shear-thinning system with coaxial mixer. *Chin. J. Chem. Eng.* **2018**, *26*, 1785–1791. [CrossRef]
19. Khalili, F.; Nasr, M.R.J.; Kazemzadeh, A.; Ein-Mozaffari, F. Hydrodynamic performance of the ASI impeller in an aerated bioreactor containing the biopolymer solution through tomography and CFD. *Chem. Eng. Res. Des.* **2017**, *125*, 190–203. [CrossRef]
20. Khalili, F.; Nasr, M.R.J.; Kazemzadeh, A.; Ein-Mozaffari, F. Analysis of gas holdup and bubble behavior in a biopolymer solution inside a bioreactor using tomography and dynamic gas disengagement techniques. *J. Chem. Technol. Biotechnol.* **2018**, *93*, 340–349. [CrossRef]
21. Liu, B.; Xiao, Q.; Gao, P.; Sunder, B.; Fan, F. Investigation of gas–liquid dispersion and mass transfer performance of wide-viscosity-range impellers in water solutions of xanthan gum. *Chem. Eng. Res. Des.* **2020**, *154*, 60–69. [CrossRef]
22. Gabelle, J.-C.; Augier, F.; Carvalho, A.; Rousset, R.; Morchain, J. Effect of Tank Size on kLa and Mixing Time in Aerated Stirred Reactors with Non-Newtonian Fluids. *Can. J. Chem. Eng.* **2011**, *89*, 1139–1153. [CrossRef]
23. Valverde, M.R.; Bettega, R.; Badino, A.C. Numerical Evaluation of Mass Transfer Coefficient in Stirred Tank Reactors with Non-Newtonian Fluid. *Theor. Found. Chem. Eng.* **2016**, *50*, 945–958. [CrossRef]
24. Wang, P.; Reviol, R.; Kluck, S.; Wurtz, P.; Bohle, M. Mixing of non-Newtonian fluids in a cylindrical stirred vessel equipped with a novel side-entry propeller. *Chem. Eng. Sci.* **2018**, *190*, 384–395. [CrossRef]
25. Kazemzadeh, A.; Elias, C.; Tamer, M.; Lohi, A.; Ein-Mozaffari, F. Mass transfer in a single-use angled-shaft aerated stirred bioreactor applicable for animal cell culture. *Chem. Eng. Sci.* **2020**, *219*, 115606. [CrossRef]
26. Auger, F.; Andre, C.; Bouvier, L.; Redl, A.; Morel, M.; Delaplace, G. Power Requirement for Mixing Shear-Thinning Fluids with a Planetary Mixer. *Chem. Eng. Technol.* **2015**, *38*, 1543–1549. [CrossRef]
27. Pakzad, L.; Ein-Mozaffari, F.; Upreti, S.R.; Lohi, A. Agitation of Herschel–Bulkley fluids with the Scaba–anchor coaxial mixers. *Chem. Eng. Res. Des.* **2013**, *91*, 761–777. [CrossRef]

28. Kazemzadeh, A.; Ein-Mozaffari, F.; Lohi, A.; Pakzad, L. A new perspective in the evaluation of the mixing of biopolymer solutions with different coaxial mixers comprising of two dispersing impellers and a wall scraping anchor. *Chem. Eng. Res. Des.* **2016**, *114*, 202–219. [CrossRef]
29. Jamshidzadeh, M.; Ein-Mozaffari, F.; Lohi, A. Local and overall gas holdup in an aerated coaxial mixing system containing a non-Newtonian fluid. *AIChE J.* **2020**, *66*, e17016. [CrossRef]
30. Jegatheeswaran, S.; Kazemzadeh, A.; Ein-Mozaffari, F. Enhanced aeration efficiency in non-Newtonian fluids using coaxial mixers: High-solidity ratio central impeller with an anchor. *Chem. Eng. J.* **2019**, *378*, 122081. [CrossRef]
31. Triveni, B.; Vishwanadham, B.; Madhavi, T.; Venkateshwar, S. Mixing studies of non-Newtonian fluids in an anchor agitated vessel. *Chem. Eng. Res. Des.* **2010**, *88*, 809–818. [CrossRef]
32. Jamshidzadeh, M.; Kazemzadeh, A.; Ein-Mozaffari, F.; Lohi, A. Analysis of power consumption for gas dispersion in non-Newtonian fluids with a coaxial mixer: New correlations for Reynolds and power numbers. *Chem. Eng. J.* **2020**, *401*, 126002. [CrossRef]
33. Jegatheeswaran, S.; Ein-Mozaffari, F. Investigation of the detrimental effect of the rotational speed on gas holdup in non-Newtonian fluids with Scaba-anchor coaxial mixer: A paradigm shift in gas-liquid mixing. *Chem. Eng. J.* **2020**, *383*, 123118. [CrossRef]
34. Bach, C.; Yang, J.; Larsson, H.; Stocks, S.M.; Gernaey, K.V.; Albaek, M.O.; Kruhne, U. Evaluation of mixing and mass transfer in a stirred pilot scale bioreactor utilizing CFD. *Chem. Eng. Sci.* **2017**, *171*, 19–26. [CrossRef]
35. Cappello, V.; Plais, C.; Vial, C.; Augier, F. Bubble size and liquid-side mass transfer coefficient measurements in aerated stirred tank reactors with non-Newtonian liquids. *Chem. Eng. Sci.* **2020**, *211*, 115280. [CrossRef]
36. Carbajal, R.I.; Tecante, A. On the applicability of the dynamic pressure step method for kLa determination in stirred Newtonian and non-Newtonian fluids, culture media and fermentation broths. *Biochem. Eng. J.* **2004**, *18*, 185–192. [CrossRef]
37. Jamshidzadeh, M.; Ein-Mozaffari, F.; Lohi, A. Experimental Analysis of the Mass Transfer Coefficient and Interfacial Area in an Aerated Coaxial Mixing System Comprising a Non-Newtonian Solution. *Ind. Eng. Chem. Res.* **2020**, *59*, 21530–21547. [CrossRef]
38. Moilanen, P.; Laakkonen, M.; Aittamaa, J. Modeling Aerated Fermenters with Computational Fluid Dynamics. *Ind. Eng. Chem. Res.* **2006**, *45*, 8656–8663. [CrossRef]
39. Luong, H.T.; Volesky, B. Mechanical Power Requirements of Gas-Liquid Agitated Systems. *AIChE J.* **1979**, *25*, 893–895. [CrossRef]
40. Gomez-Diaz, D.; Navaza, J.M. Analysis of carbon dioxide gas/liquid mass transfer in aerated stirred vessels using non–Newtonian media. *J. Chem. Technol. Biotechnol.* **2004**, *79*, 1105–1112. [CrossRef]
41. Michel, B.J.; Miller, S.A. Power Requirements of Gas-Liquid Agitated Systems. *AIChE J.* **1962**, *8*, 262–266. [CrossRef]
42. Xie, M.; Xia, J.; Zhou, Z.; Zhou, G.; Chu, J.; Zhuang, Y.; Zhang, S.; Noorman, H. Power consumption, local and average volumetric mass transfer coefficient in multiple-impeller stirred bioreactors for xanthan gum solutions. *Chem. Eng. Sci.* **2014**, *106*, 144–156. [CrossRef]
43. Lee, B.W.; Dudukovic, M.P. Time-series analysis of optical probe measurements in gas–liquid stirred tank. *Chem. Eng. Sci.* **2014**, *116*, 623–634. [CrossRef]
44. Xiao, Y.; Li, X.; Ren, S.; Mao, Z.; Yang, C. Hydrodynamics of gas phase under typical industrial gassing rates in a gas-liquid stirred tank using intrusive image-based method. *Chem. Eng. Sci.* **2020**, *227*, 115923. [CrossRef]
45. Bao, Y.; Chen, L.; Gao, Z.; Chen, J. Local void fraction and bubble size distributions in cold-gassed and hot-sparged stirred reactors. *Chem. Eng. Sci.* **2010**, *65*, 976–984. [CrossRef]
46. Laakkonen, M.; Honkanen, M.; Saarenrinne, P.; Aittamaa, J. Local bubble size distributions, gas–liquid interfacial areas and gas holdups in a stirred vessel with particle image velocimetry. *Chem. Eng. J.* **2005**, *109*, 37–47. [CrossRef]
47. Liu, Y.; Li, W.; Han, L.; Cao, Y.; Luo, H.; Al-Dahhan, M.; Dudukovic, M.P. γ-CT measurement and CFD simulation of cross section gas holdup distribution in a gas–liquid stirred standard Rushton tank. *Chem. Eng. Sci.* **2011**, *66*, 3721–3731. [CrossRef]
48. Wang, M.; Dorward, A.; Vlaev, D.; Mann, R. Measurements of gas–liquid mixing in a stirred vessel using electrical resistance tomography (ERT). *Chem. Eng. J.* **2000**, *77*, 93–98. [CrossRef]
49. Jamshidzadeh, M.; Kazemzadeh, A.; Ein-Mozaffari, F.; Lohi, A. Intensification of gas dispersion in pseudoplastic fluids with coaxial mixers. *Chem. Eng. Process.* **2020**, *155*, 108058. [CrossRef]
50. Mavros, P. Flow Visualization in Stirred Vessels: A Review of Experimental Techniques. *Chem. Eng. Res. Des.* **2001**, *79*, 113–127. [CrossRef]
51. Machon, V.; Vlcek, J.; Nienow, A.W.; Solomon, J. Some Effects of Pseudoplasticity on Hold-up in Aerated, Agitated Vessels. *Chem. Eng. J.* **1980**, *19*, 67–74. [CrossRef]
52. Kudrewizki, F.; Rabe, P. Model of the Dissipation of Mechanical Energy in Gassed Stirred Tanks. *Chem. Eng. Sci.* **1986**, *41*, 2247–2252. [CrossRef]
53. Garcia-Ochoa, F.; Gomez, E. Bioreactor scale-up and oxygen transfer rate in microbial processes: An overview. *Biotechnol. Adv.* **2009**, *27*, 153–176. [CrossRef] [PubMed]
54. Gogate, P.R.; Pandit, A.B. Survey of measurement techniques for gas–liquid mass transfer coefficient in bioreactors. *Biochem. Eng. J.* **1999**, *4*, 7–15. [CrossRef]
55. Garcia-Ochoa, F.; Gomez, E. Theoretical prediction of gas–liquid mass transfer coefficient, specific area and hold-up in sparged stirred tanks. *Chem. Eng. Sci.* **2004**, *59*, 2489–2501. [CrossRef]

56. Pinelli, D.; Liu, Z.; Magelli, F. Analysis of kLa Measurement Methods in Stirred Vessels: The Role of Experimental Techniques and Fluid Dynamic Models. *Int. J. Chem. React.* **2010**, *8*, A115. [CrossRef]
57. Moucha, T.; Rejl, F.J.; Kordač, M.; Labík, L. Mass transfer characteristics of multiple-impeller fermenters for their design and scale-up. *Biochem. Eng. J.* **2012**, *69*, 17–27. [CrossRef]
58. Petricek, R.; Moucha, T.; Kacrík, T.; Rejl, F.J.; Valenz, L.; Haidl, J. Volumetric mass transfer coefficient in the fermenter agitated by Rushton turbines of various diameters in coalescent batch. *Int. J. Heat Mass Transf.* **2019**, *130*, 968–977. [CrossRef]
59. Scargiali, F.; Busciglio, A.; Grisafi, F.; Brucato, A. Simplified dynamic pressure method for kLa measurement in aerated bioreactors. *Biochem. Eng. J.* **2010**, *49*, 165–172. [CrossRef]
60. Yang, J.D.; Wang, N.S. Oxygen Mass Transfer Enhancement via Fermentor Headspace Pressurization. *Biotechnol. Prog.* **1992**, *8*, 244–251. [CrossRef]
61. Pan, A.; Xie, M.; Xia, J.; Chu, J.; Zhuang, Y. Gas-liquid mass transfer studies: The influence of single- and double-impeller configurations in stirred tanks. *Korean J. Chem. Eng.* **2018**, *35*, 61–72. [CrossRef]
62. Vasconcelos, J.M.T.; Nienow, A.W.; Martin, T.; Alves, S.S.; McFarlane, C.M. Alternative Ways of Applying the Hydrogen Peroxide Steady State Method of kLa Measurement. *Chem. Eng. Res. Des.* **1997**, *75*, 467–472. [CrossRef]
63. Ortiz-Ochoa, K.; Doig, S.D.; Ward, J.M.; Baganz, F. A novel method for the measurement of oxygen mass transfer rates in small-scale vessels. *Biochem. Eng. J.* **2005**, *25*, 63–68. [CrossRef]
64. Garcia-Ochoa, F.; Castro, E.G.; Santos, V.E. Oxygen transfer and uptake rates during xanthan gum production. *Enzyme Microb. Technol.* **2000**, *27*, 680–690. [CrossRef]
65. Momiroski, V.; Bhattacharya, S.; Davoody, M.; Raman, A.A.B.A.; Parthasarathy, R. Size distribution of bubbles in agitated viscous Newtonian and non-Newtonian solutions. *Asia-Pac. J. Chem. Eng.* **2018**, *13*, e2267. [CrossRef]
66. Alves, S.S.; Maia, C.I.; Vasconcelos, J.M.T.; Serralheiro, A.J. Bubble size in aerated stirred tanks. *Chem. Eng. J.* **2002**, *89*, 109–117. [CrossRef]
67. De Figueiredo, M.M.L. The Physical and Mass Transfer Properties of Gas Dispersion in Mixing Vessels. Doctoral Thesis, University of Edinburg, Edinburgh, UK, 1978.
68. Gao, Z.; Smith, J.M.; Muller-Steinhagen, H. Void fraction distribution in sparged and boiling reactors with modern impeller configuration. *Chem. Eng. Process.* **2001**, *40*, 489–497. [CrossRef]
69. Honkanen, M.; Eloranta, H.; Saarenrinne, P. Digital imaging measurement of dense multiphase flows in industrial processes. *Flow Meas. Instrum.* **2010**, *21*, 25–32. [CrossRef]
70. Barigou, M.; Greaves, M. A capillary suction probe for bubble size measurement. *Meas. Sci. Technol.* **1991**, *2*, 318–326. [CrossRef]
71. Barigou, M.; Greaves, M. Bubble-size Distributions in a Mechanically Agitated Gas-liquid Contactor. *Chem. Eng. Sci.* **1992**, *47*, 2009–2025. [CrossRef]
72. Kamiwano, M.; Kaminoyama, M.; Nishi, K.; Shirota, D. A Method for Measuring Bubble Diameter Distribution in Gas-Liquid Agitated Vessel under High Gas Hold-Up Using Real-Time High-Speed Image Processing System. *J. Chem. Eng. Jpn.* **1998**, *31*, 366–373. [CrossRef]
73. Bouaifi, M.; Roustan, M. Bubble Size and Mass Transfer Coefficients in Dual-Impeller Agitated Reactors. *Can. J. Chem. Eng.* **1998**, *76*, 390–397. [CrossRef]
74. Busciglio, A.; Grisafi, F.; Scargiali, F.; Brucato, A. On the measurement of local gas hold-up, interfacial area and bubble size distribution in gas–liquid contactors via light sheet and image analysis: Imaging technique and experimental results. *Chem. Eng. Sci.* **2013**, *102*, 551–566. [CrossRef]
75. Hashemi, N.; Ein-Mozaffari, F.; Upreti, S.R.; Hwang, D.K. Experimental investigation of the bubble behavior in an aerated coaxial mixing vessel through electrical resistance tomography (ERT). *Chem. Eng. J.* **2016**, *289*, 402–412. [CrossRef]
76. Calderbank, P.H. Physical rate processes in industrial fermentation. Part I: The interfacial area in gas-liquid contacting with mechanical agitation. *Trans. Inst. Chem. Eng.* **1958**, *35*, 442–463.
77. Bhavaraju, S.M.; Russel, T.W.F.; Blanck, H.W. The Design of Gas Sparged Devices for Viscous Liquid Systems. *AIChE J.* **1978**, *24*, 454–466. [CrossRef]
78. Wang, W.; Mao, Z.; Yang, C. Experimental and Numerical Investigation on Gas Holdup and Flooding in an Aerated Stirred Tank with Rushton Impeller. *Ind. Eng. Chem. Res.* **2006**, *45*, 1141–1151. [CrossRef]
79. Paglianti, A. Simple Model to Evaluate Loading/Flooding Transition in Aerated Vessels Stirred by Rushton Disc Turbines. *Can. J. Chem. Eng.* **2002**, *80*, 1–5. [CrossRef]
80. Warmoeskerken, M.M.C.G.; Smith, J.M. Flooding of Disc Turbines in Gas-Liquid Dispersions: A New Description of the Phenomenon. *Chem. Eng. Sci.* **1985**, *40*, 2063–2071. [CrossRef]
81. Aubin, J.; Le Sauze, N.; Bertrand, J.; Fletcher, D.F.; Xuereb, C. PIV measurements of flow in an aerated tank stirred by a down- and an up-pumping axial flow impeller. *Exp. Therm. Fluid Sci.* **2004**, *28*, 447–456. [CrossRef]
82. Montante, G.; Paglianti, A. Gas hold-up distribution and mixing time in gas–liquid stirred tanks. *Chem. Eng. J.* **2015**, *279*, 648–658. [CrossRef]
83. Warmoeskerken, M.M.C.G.; Speur, J.; Smith, J.M. Gas-liquid Dispersion with Pitched Blade Turbines. *Chem. Eng. Commun.* **1984**, *25*, 11–29. [CrossRef]
84. Rosseburg, A.; Fitschen, J.; Wutz, J.; Wucherpfennig, T.; Schlüter, M. Hydrodynamic inhomogeneities in large scale stirred tanks—Influence on mixing time. *Chem. Eng. Sci.* **2018**, *188*, 208–220. [CrossRef]

85. Paglianti, A.; Fujasova, M.; Montante, G. A Simple Model for Power Consumption in Gassed and Boiling Stirred Vessels. *AIChE J.* **2008**, *54*, 646–656. [CrossRef]
86. Nienow, A.W. Hydrodynamics of stirred bioreactors. *Appl. Mech. Rev.* **1998**, *51*, 3–32. [CrossRef]
87. Evans, G.M.; Manning, S.A.; Jameson, G.J. Cavity Formation, Growth, and Dispersion behind Rotating Impeller Blades. *Ind. Eng. Chem. Res.* **2005**, *44*, 6304–6309. [CrossRef]
88. Cabaret, F.; Fradette, L.; Tanguy, P.A. Gas–liquid mass transfer in unbaffled dual-impeller mixers. *Chem. Eng. Sci.* **2008**, *63*, 1636–1647. [CrossRef]
89. Hassan, R.; Loubiere, K.; Legrand, J.; Delaplace, G. A consistent dimensional analysis of gas–liquid mass transfer in an aerated stirred tank containing purely viscous fluids with shear-thinning properties. *Chem. Eng. J.* **2012**, *184*, 42–56. [CrossRef]
90. Nienow, A.W.; Wisdom, D.J.; Solomon, J. The effect of rheological complexities on power consumption in an aerated, agitated vessel. *Chem. Eng. Commun.* **1983**, *19*, 273–293. [CrossRef]
91. McFarlane, C.M.; Nienow, A.W. Studies of High Solidity Ratio Hydrofoil Impellers for Aerated Bioreactors. 1. Review. *Biotechnol. Prog.* **1995**, *11*, 601–607. [CrossRef]
92. Amanullah, A.; Tuttiett, B.; Nienow, A.W. Agitator Speed and Dissolved Oxygen Effects in Xanthan Fermentations. *Biotechnol. Bioeng.* **1997**, *57*, 198–210. [CrossRef]
93. Pakzad, L.; Ein-Mozaffari, F.; Chan, P. Using electrical resistance tomography and computational fluid dynamics modeling to study the formation of cavern in the mixing of pseudoplastic fluids possessing yield stress. *Chem. Eng. Sci.* **2008**, *63*, 2508–2522. [CrossRef]
94. Ameur, H.; Vial, C. Modified scaba 6SRGT impellers for process intensification: Cavern size and energy saving when stirring viscoplastic fluids. *Chem. Eng. Process.* **2020**, *148*, 107795. [CrossRef]
95. Yagi, H.; Yoshida, F. Gas Absorption by Newtonian and Non-Newtonian Fluids in Sparged Agitated Vessels. *Ind. Eng. Chem. Process. Des. Dev.* **1975**, *14*, 488–493. [CrossRef]
96. Solomon, J.; Elpson, T.P.; Nienow, A.W.; Pace, G.W. Cavern Sizes in Agitated Fluids with a Yield Stress. *Chem. Eng. Commun.* **1981**, *11*, 143–164. [CrossRef]
97. Moilanen, P.; Laakkonen, M.; Visuri, O.; Aittamaa, J. Modeling Local Gas-Liquid Mass Transfer in Agitated Viscous Shear-Thinning Dispersions with CFD. *Ind. Eng. Chem. Res.* **2007**, *46*, 7289–7299. [CrossRef]
98. Karimi, A.; Golbabaei, F.; Mehrnia, M.R.; Neghab, M.; Mohammad, K.; Nikpey, A.; Pourmand, M.R. Oxygen mass transfer in a stirred tank bioreactor using different impeller configurations for environmental purposes. *Iran. J. Environ. Health Sci. Eng.* **2013**, *10*, 6. [CrossRef]
99. Jakobsen, H.A. *Chemical Reactor Modeling: Multiphase Reactive Flows*, 2nd ed.; Springer Science & Business Media: Berlin/Heidelberg, Germany, 2014. [CrossRef]
100. Buffo, M.M.; Correa, L.J.; Esperanca, M.N.; Cruz, A.J.G.; Farinas, C.S.; Badino, A.C. Influence of dual-impeller type and configuration on oxygen transfer, power consumption, and shear rate in a stirred tank bioreactor. *Biochem. Eng. J.* **2016**, *114*, 130–190. [CrossRef]
101. Jegatheeswaran, S.; Ein-Mozaffari, F. Use of Gas Helicity as an Indicator to Evaluate Impeller Design and its Gas Holdup: Proof of Concept for the Intensification of Gas-Liquid Mixing. *Chem. Eng. Process.* **2020**, *156*, 108091. [CrossRef]
102. Tecante, A.; Choplin, L. Gas-Liquid Mass Transfer in Non-Newtonian Fluids in a Tank Stirred with a Helical Ribbon Screw Impeller. *Can. J. Chem. Eng.* **1993**, *71*, 859–865. [CrossRef]
103. Cheng, J.; Carreau, P.J. Aerated Mixing of Viscoelastic Fluids with Helical Ribbon Impellers. *Chem. Eng. Sci.* **1994**, *49*, 1965–1972. [CrossRef]
104. Merchuk, J.C. Shear Effects on Suspended Cells. *Adv. Biochem. Engin. Biotechnol.* **1991**, *44*, 65–95. [CrossRef]
105. Jiang, J.; Wu, J.; Poncin, S.; Li, H.Z. Effect of hydrodynamic shear on biogas production and granule characteristics in a continuous stirred tank reactor. *Process Biochem.* **2016**, *51*, 345–351. [CrossRef]
106. Khare, A.S.; Niranjan, K. The effect of impeller design on gas hold-up in surfactant containing highly viscous non-Newtonian agitated liquids. *Chem. Eng. Process.* **2002**, *41*, 239–249. [CrossRef]
107. Ghotli, R.A.; Aziz, A.R.A.; Ibrahim, S.; Baroutian, S.; Arami-Niya, A. Study of various curved-blade impeller geometries on power consumption in stirred vessel using response surface methodology. *J. Taiwan Inst. Chem. Eng.* **2013**, *44*, 192–201. [CrossRef]
108. Garcia-Ochoa, F.; Gomez, E. Mass transfer coefficient in stirred tank reactors for xanthan gum solutions. *Biochem. Eng. J.* **1998**, *1*, 1–10. [CrossRef]
109. Ranade, V.R.; Ulbrecht, J.J. Influence of Polymer Additives on the Gas-Liquid Mass Transfer in Stirred Tanks. *AIChE J.* **1978**, *24*, 796–803. [CrossRef]
110. Ali, H.; Solsvik, J. Axial distributions of bubble–liquid mass transfer coefficient in laboratory-scale stirred tank with viscous Newtonian and non-Newtonian fluids. *Phys. Fluids* **2020**, *32*, 123308. [CrossRef]
111. Ogut, A.; Hatch, R.T. Oxygen Transfer into Newtonian and Non-Newtonian Fluids in Mechanically Agitated Vessels. *Can. J. Chem. Eng.* **1988**, *66*, 79–85. [CrossRef]
112. Khopkar, A.R.; Kasat, G.R.; Pandit, A.B.; Ranade, V.V. CFD Simulation of mixing in tall gas-liquid stirred vessel: Role of local flow patterns. *Chem. Eng. Sci.* **2006**, *61*, 2921–2929. [CrossRef]
113. Gogate, P.R.; Beenackers, A.A.C.M.; Pandit, A.B. Multiple-impeller systems with a special emphasis on bioreactors: A critical review. *Biochem. Eng. J.* **2000**, *6*, 109–144. [CrossRef]

114. Takahashi, K.; Yokota, T.; Konno, H. Mixing of Pseudoplastic Liquid in a Vessel Equipped with a Variety of Helical Ribbon Impellers. *J. Chem. Eng. Jpn.* **1988**, *21*, 63–68. [CrossRef]
115. Amiraftabi, M.; Khiadani, M.; Mohammed, H.A. Performance of a dual helical ribbon impeller in a two-phase (gas-liquid) stirred tank reactor. *Chem. Eng. Process.* **2020**, *148*, 107811. [CrossRef]
116. Suhaili, N.; Mohamed, M.S.; Mohamad, R.; Ariff, A.B. Gas-liquid Mass Transfer Performance of Dual Impeller System Employing Rushtons, Concave-bladed Disc (CD-6) Turbines and Their Combination in Stirred Tank Bioreactor. *J. Appl. Sci. Res.* **2010**, *6*, 234–244.
117. Liu, B.; Zhang, Y.; Chen, M.; Li, P.; Jin, Z. Power consumption and flow field characteristics of a coaxial mixer with a double inner impeller. *Chin. J. Chem. Eng.* **2015**, *23*, 1–6. [CrossRef]
118. Tanguy, P.A.; Thibault, F. Power Consumption in the Turbulent Regime for a Coaxial Mixer. *Can. J. Chem. Eng.* **2002**, *80*, 601–603. [CrossRef]
119. Rudolph, L.; Schafer, M.; Atiemo-Obeng, V.; Kraume, M. Experimental and Numerical Analysis of Power Consumption for Mixing of High Viscosity Fluids with a Co-axial Mixer. *Chem. Eng. Res. Des.* **2007**, *85*, 568–575. [CrossRef]
120. Hashemi, N.; Ein-Mozaffari, F.; Upreti, S.R.; Hwang, D.K. Analysis of mixing in an aerated reactor equipped with the coaxial mixer through electrical resistance tomography and response surface method. *Chem. Eng. Res. Des.* **2016**, *109*, 734–752. [CrossRef]
121. Espinosa-Solares, T.; Brito-De la Fuente, E.; Tecante, A.; Tanguy, P.A. Gas Dispersion in Rheologically-Evolving Model Fluids by Hybrid Dual Mixing Systems. *Chem. Eng. Technol.* **2002**, *25*, 723–727.
122. Espinosa-Solares, T.; Brito-De la Fuente, E.; Tecante, A.; Medina-Torres, L.; Tanguy, P.A. Mixing Time in Rheologically Evolving Model Fluids by Hybrid Dual Mixing Systems. *Chem. Eng. Res. Des.* **2002**, *80*, 817–823. [CrossRef]
123. Liu, B.; Huang, B.; Zhang, Y.; Liu, J.; Jin, Z. Numerical study on gas dispersion characteristics of a coaxial mixer with viscous fluids. *J. Taiwan Inst. Chem. Eng.* **2016**, *66*, 54–61. [CrossRef]
124. Cascaval, D.; Galaction, A.; Turnea, M. Comparative analysis of oxygen transfer rate distribution in stirred bioreactor for simulated and real fermentation broths. *J. Ind. Microbiol. Biotechnol.* **2011**, *38*, 1449–1466. [CrossRef]
125. Bombac, A.; Zumer, M.; Zun, I. Power Consumption in Mixing and Aerating of Shear Thinning Fluid in a Stirred Vessel. *Chem. Biochem. Eng. Q.* **2007**, *21*, 131–138.
126. Campesi, A.; Cerri, M.O.; Hokka, C.O.; Badino, A.C. Determination of the average shear rate in a stirred and aerated tank bioreactor. *Bioprocess Biosyst. Eng.* **2009**, *32*, 241–248. [CrossRef] [PubMed]
127. Liu, B.; Xiao, Q.; Sun, N.; Gao, P.; Fan, F.; Sunden, B. Effect of gas distributor on gas–liquid dispersion and mass transfer characteristics in stirred tank. *Chem. Eng. Res. Des.* **2019**, *145*, 314–322. [CrossRef]
128. Perez, J.A.S.; Porcel, E.M.R.; Lopez, J.L.C.; Sevilla, J.M.F.; Chisti, Y. Shear rate in stirred tank and bubble column bioreactors. *Chem. Eng. J.* **2006**, *124*, 1–5. [CrossRef]
129. Metzner, A.B.; Otto, R.E. Agitation of non-Newtonian fluids. *AIChE J.* **1957**, *3*, 3–10. [CrossRef]
130. Gabelle, J.-C.; Morchain, J.; Anne-Archard, D.; Augier, F.; Line, A. Experimental Determination of the Shear Rate in a Stirred Tank with a Non-Newtonian Fluid: Carbopol. *AIChE J.* **2013**, *59*, 2251–2266. [CrossRef]
131. Calderbank, P.H.; Moo-Young, M.B. The prediction of power consumption in the agitation of non-Newtonian fluids. *Chem. Eng. Res. Des.* **1959**, *37*, 26–33.
132. Park, S.; Sohn, I.; Park, D.; Oh, K. Absorption of Carbon Dioxide into Non-Newtonian Liquid. I. Effect of Viscoelasticity. *Sep. Sci. Technol.* **2003**, *38*, 1361–1384. [CrossRef]
133. Vlaev, S.D.; Valeva, M.D.; Mann, R. Some effects of rheology on the spatial distribution of gas hold-up in a mechanically agitated vessel. *Chem. Eng. J.* **2002**, *87*, 21–30. [CrossRef]
134. Kerdouss, F.; Bannari, A.; Proulx, P.; Bannari, R.; Skrga, M.; Labrecque, Y. Two-phase mass transfer coefficient prediction in stirred vessel with a CFD model. *Comput. Chem. Eng.* **2008**, *32*, 1943–1955. [CrossRef]
135. Guan, X.; Li, X.; Yang, N.; Liu, M. CFD simulation of gas-liquid flow in stirred tanks: Effect of drag models. *Chem. Eng. J.* **2020**, *386*, 121554. [CrossRef]
136. Sajjadi, B.; Raman, A.A.A.; Ibrahim, S.; Shah, R.S.S.R.E. Review on gas-liquid mixing analysis in multiscale stirred vessel using CFD. *Rev. Chem. Eng.* **2012**, *28*, 171–189. [CrossRef]
137. Bao, Y.; Yang, J.; Chen, L.; Gao, Z. Influence of the Top Impeller Diameter on the Gas Dispersion in a Sparged Multi-impeller Stirred Tank. *Ind. Eng. Chem. Res.* **2012**, *51*, 12411–12420. [CrossRef]
138. Scargiali, F.; D'Orazio, A.; Grisafi, F.; Brucato, A. Modelling and Simulation of Gas-Liquid Hydrodynamics in Mechanically Stirred Tanks. *Chem. Eng. Res. Des.* **2007**, *85*, 637–646. [CrossRef]
139. Tzounakos, A.; Karamanev, D.G.; Margaritis, A.; Bergougnou, M.A. Effect of the surfactant concentration on the rise of gas bubbles in power-law non-Newtonian liquids. *Ind. Eng. Chem. Res.* **2004**, *43*, 5790–5795. [CrossRef]
140. Amiraftabi, M.; Khiadani, M.; Mohammed, H.A.; Arshad, A. CFD-PBM and experimental investigation of a shear thinning fluid in a gas-liquid tank agitated by a helical ribbon impeller. *Sep. Purif. Technol.* **2021**, *272*, 118855. [CrossRef]
141. Oosterhuis, N.M.G. Scale-Up of Bioreactors: A Scale-Down Approach. Doctoral Thesis, Delft University of Technology, Delft, The Netherlands, 1984.
142. Martin, M.; Montes, F.J.; Galán, M.A. Physical explanation of the empirical coefficients of gas–liquid mass transfer equations. *Chem. Eng. Sci.* **2009**, *64*, 410–425. [CrossRef]

143. Nauha, E.K.; Visuri, O.; Vermasvuori, R.; Alopaeus, V. A new simple approach for the scale-up of aerated stirred tanks. *Chem. Eng. Res. Des.* **2015**, *95*, 150–161. [CrossRef]
144. Qu, L.; Ren, L.; Huang, H. Scale-up of docosahexaenoic acid production in fed-batch fermentation by *Schizochytrium* sp. based on volumetric oxygen-transfer coefficient. *Biochem. Eng. J.* **2013**, *77*, 82–87. [CrossRef]
145. Hardy, N.; Augier, F.; Nienow, A.W.; Béal, C.; Chaabane, F.B. Scale-up agitation criteria for *Trichoderma reesei* fermentation. *Chem. Eng. Sci.* **2017**, *172*, 158–168. [CrossRef]
146. Maluta, F.; Paglianti, A.; Montante, G. Two-fluids RANS predictions of gas cavities, power consumption, mixing time and oxygen transfer rate in an aerated fermenter scale-down stirred with multiple impellers. *Biochem. Eng. J.* **2021**, *166*, 107867. [CrossRef]